# Measured Boundary Layer Transition and Rotor Hover Performance at Model Scale

Austin D. Overmeyer,[*] and Dr. Preston B. Martin [†]

*U.S. Army Aviation Development Directorate (ADD)*

*NASA Langley Research Center, Hampton, VA 23681*

An experiment involving a Mach-scaled, $11.08\ ft.$ diameter rotor was performed in hover during the summer of 2016 at NASA Langley Research Center. The experiment investigated the hover performance as a function of the laminar to turbulent transition state of the boundary layer, including both natural and fixed transition cases. The boundary layer transition locations were measured on both the upper and lower aerodynamic surfaces simultaneously. The measurements were enabled by recent advances in infrared sensor sensitivity and stability. The infrared thermography measurement technique was enhanced by a paintable blade surface heater, as well as a new high-sensitivity long wave infrared camera. The measured transition locations showed extensive amounts, $x/c > 0.90$, of laminar flow on the lower surface at moderate to high thrust ($C_T/\sigma > 0.068$) for the full blade radius. The upper surface showed large amounts, $x/c > 0.50$, of laminar flow at the blade tip for low thrust ($C_T/\sigma < 0.045$). The objective of this paper is to provide an experimental data set for comparisons to newly developed and implemented rotor boundary layer transition models in CFD and rotor design tools. The data is expected to be used as part of the AIAA Rotorcraft Simulation Working Group.

## Nomenclature

| | |
|---|---|
| $14x22$ | 14- by 22-Foot Subsonic Tunnel |
| $GRMS$ | General Rotor Model System |
| $LWIR$ | Long Wave Infrared |
| $RTC$ | Rotor Test Cell |
| | |
| $c$ | chord, *in* |
| $C_P$ | power coefficient |
| $C_T$ | thrust coefficient |
| $FM$ | figure of merit |
| $h$ | trip dot height, *in* |
| $M$ | Mach number |
| $PA$ | ambient pressure, *psf* |
| $r$ | radial coordinate, *in* |
| $R$ | rotor radius, *in* |
| $R_a$ | average surface roughness, *μin* |
| $Re$ | Reynolds number |
| $Re_{tr}$ | Reynolds number at transition |
| $TA$ | ambient temperature, *degF* |
| $x$ | chordwise coordinate, *in* |
| $x_{tr,l-0.65}$ | Transition location, x/c, lower surface, r/R=0.65 |
| $x_{tr,l-0.72}$ | Transition location, x/c, lower surface, r/R=0.72 |
| $x_{tr,l-0.90}$ | Transition location, x/c, lower surface, r/R=0.90 |
| $x_{tr,u-0.65}$ | Transition location, x/c, upper surface, r/R=0.65 |

---

[*]Research Scientist, NASA Langley Research Center, Hampton ,VA 23681

[†]Sr. Research Scientist, NASA Langley Research Center, Hampton ,VA 23681

American Institute of Aeronautics and Astronautics

$x_{tr,u-0.72}$  Transition location, x/c, upper surface, r/R=0.72
$x_{tr,u-0.90}$  Transition location, x/c, upper surface, r/R=0.90

$\rho$       air density, $slug/ft^3$
$\sigma$       area weighted solidity

# I.    Introduction

The prediction of rotorcraft hover performance remains a technical challenge for the rotorcraft community. The challenge, in part, is due to a lack of a comprehensive validation data set for comparison to predictions. While this paper does not present such a data set, it begins to provide a better understanding of the measurements required to establish a validation data set, especially in detailing the importance of tracking the transition location on the upper and lower aerodynamic surfaces of the blades.

As a result, the key contribution of the present work is detailed measurements of the boundary layer transition locations as a function of rotor thrust. Measuring transition on rotor blades is nothing new, and the work of Boatwright et al., Ref. 1 serves as an excellent early (1974) example of an attempt to understand how much laminar flow exists on a full-scale rotor (in this case using chemical sublimation flow visualization). At model scale, the visualization of laminar separation and forced transition was done using oil flow, sublimation, and liquid crystals by Martin, Ref. 2. These early efforts typically showed extensive amounts of laminar flow developing at both model and full scale. Recent advances in IR thermography led to the tests in 2014 and 2016 by Richter et al., Ref. 3, 4. The 2016 paper detailed the boundary layer transition locations over the rotor radius at full-scale in hover. The test by Richter also measured extensive amounts of laminar flow on the lower surface of a full-scale BK-117-type rotor in hover. Aside from these tests only a limited amount of research has been performed in the prior years to measure laminar flow on a rotor, see Refs. 5–7. In comparison, a significant amount of research has been focused on induced power reduction through planform variation. In part, the limited amount of rotor laminar flow research is due to the notion that high free-stream turbulence and blade surface roughness due to manufacturing tolerances and erosion would prevent laminar flow from being achieved in flight. While these are many of the same challenges faced by the fixed-wing aerodynamics community, the rotor blade boundary layer has additional factors to consider, such as large spanwise variation of twist, Reynolds and Mach numbers, and airfoil shape. At model-scale with fairly low Reynolds numbers on the inboard part of the blade, laminar separation bubbles can force early transition. At full-scale, the higher Reynolds numbers at the tip may cause early transition and less laminar flow at full-scale than at model-scale. These competing Reynolds number effects require that the boundary layer state be measured for the full blade radius during hover performance tests for all scales.

The objective of this paper is to provide a preliminary experimental data set of boundary layer transition locations for comparisons to newly developed and implemented rotor transition models in CFD. The paper presents experimental transition locations of a model scale rotor measured via an improved infrared (IR) thermography technique. The improved IR thermography technique utilizes a paint-based heater coating to generate the temperature differential required to measure the transition locations. As a proof of concept, the heater coating was retrofitted to the existing blade surface. While the surface coating was thin, approximately 2-3 mils thick, the buss bars on the trailing edge roughly tripled the trailing-edge thickness. As a result, the transition locations presented in this paper shall be treated as preliminary data used to identify the transition characteristics and global trends.

# II.    Test Overview

A Mach-scale hover test was conducted in the NASA LaRC Rotor Test Cell (RTC) during the Summer of 2016. Boundary layer transition locations were acquired on the upper and lower aerodynamic surfaces simultaneously via IR thermography. The hover performance was measured for natural and forced transition cases.

## A.   Test Setup

The RTC is a large chamber measuring 40 ft wide, 68 ft long and 43 ft tall that is part of the NASA 14- by 22-Foot Subsonic Tunnel facility. The test used the General Rotor Model System (GRMS), a rotor drive system that can be fully enclosed within a fuselage shell. As described by Murrill (Ref. 8), the system is powered by two 75 hp water-cooled variable frequency electric motors and is capable of driving a rotor up to a 13.2 ft diameter through either a 5.47:1

American Institute of Aeronautics and Astronautics

high-speed transmission or a 6.90:1 low-speed transmission. Cooling for the motors is provided by an external water chiller, and lubrication for the transmission is supplied from an external lube cart. Two internal six-component strain gage force and moment balances are used for measuring the fuselage and rotor aerodynamic loads independently. The NASA T2.5MKXXX rotor balance was used to measure the six-component rotor loads. The balance specifications are given in Table 1. The first order thrust and torque are measured by the normal force and yawing moment balance components. Based on the balance calibration accuracies, the accuracy of rotor figure of merit is calculated to be $\pm 0.005 - 0.010$ depending on the measured dimensional thrust and torque.

**Table 1. NASA LaRC T2.5MK XXX limits and accuracy. The accuracy is stated as a percentage of full scale at 95% confidence.**

| Force/Moment | Calibration Full Scale (lb) or (in-lb) | Accuracy (% Full Scale) |
|---|---|---|
| Normal (Thrust) | $\pm 1000$ | 0.25 |
| Axial | $\pm 500$ | 0.46 |
| Pitch | $\pm 11091$ | 0.15 |
| Roll | $\pm 4323$ | 0.20 |
| Yaw (Torque) | $\pm 7922$ | 0.17 |
| Side | $\pm 300$ | 0.76 |

The GRMS was installed using a sting-mounted configuration, employing a dogleg adapter that was enclosed in the fuselage to attach to a long support sting. A schematic of test setup is shown in Figs. 1-2. An image of the test setup is provided in Fig. 3. The sting was mounted in a cantilevered manner to the movable mast installed in a facility model cart. The horizontal distance from the fore and aft walls was 28 and 40 ft, respectively. The side walls were 20 ft from the rotor axis. The model cart was powered such that the vertical mast supporting the sting could raise, lower and pitch, permitting nondimensional rotor height values between 2.10 and 3.89 z/R to be achieved while holding the rotor disk parallel to the floor surface. During this test, a fixed height of z/R = 3.15 (17.5 $ft$) was tested.

## B. Rotor Blades

A four-bladed fully articulated hub with a 66.50 inch rotor radius was used for this test. The rotor was operated at 1150 RPM, giving a tip velocity of 666 ft/s (Mach 0.58, which is close to where a typical helicopter rotor tip operates at 6000 feet pressure altitude 95 degrees F). The rotor blades were acquired specifically for a Pressure Sensitive Paint (PSP) validation test and were used in a previous hover test by Wong et al., see Ref. 9. The blade used Government RC-series airfoils with the planform shown in Figure 4. The rotor had a linear twist of -14 degrees starting at $r/R = 0.252$ and ending at the rotor tip. The blade had a chord length of 5.45 inches with a 30 degree tip sweep and a 3.27 inch tip chord length. The blade characteristics are summarized in Table 2. Inboard of $r/R = 0.252$, a connector fairing is used to accommodate wiring from dynamic pressure sensors within two pressure instrumented blades and is present on all four blades for symmetry. The flap and lead/lag hinges are colocated 3.00 inches from the hub center.

**Table 2. PSP Rotor Blade Characteristics.**

| | |
|---|---|
| Rotational Speed (RPM) | 1150 |
| Number of Blades | 4 |
| Blade Radius (in) | 66.50 |
| Blade Chord (in) | 5.45 |
| Rotor Airfoil | RC series |
| Blade Twist Distribution | Linear |
| Blade Twist (deg) | -14 |
| Tip Speed (ft/s) | 666 |
| Hover tip Mach number | 0.58 |
| Rotor Area Solidity ($\sigma$) | 0.1033 |

For the forced transition cases, trip dots were placed at $x/c = 0.05$ on the upper and lower surface. The dots had a diameter of 0.050 inches and a spacing of 0.100 inches. The trip dot height was varied as a function of rotor radius

American Institute of Aeronautics and Astronautics

to force transition and to minimize device drag. From $r/R = 0.25 - 0.50$ the trip height was $h = 9.9$ *mils* and from $r/R = 0.50 - 1.00$ the trip height was $h = 5.0$ *mils*. The installation of the trip dots is shown on the lower surface in Figs. 5 and 6 for the root and tip sections of the blade, respectively. The surface roughness of the blades was measured using a portable stylus trace. The trace distance for each measurement was 0.1 inches in the chordwise direction. The average blade surface roughness of 15 locations was measured to be $R_a = 30$ *µin*.

## C.  Infrared Thermography Setup

The boundary layer transition locations were measured using IR thermography. IR thermography requires a temperature differential between the aerodynamic surface and the ambient flow. The difference in heat transfer rate between a laminar and turbulent boundary layer results in a slightly different surface temperature, which can be detected by an IR camera of sufficient sensitivity. To create the temperature differential, one of the four blades was retrofitted with a urethane paint-based highly conductive coating to serve as a heater. The heater was divided into two spanwise zones and powered through a slip ring by a power supply in the fixed frame. The heating zones could be independently controlled to provide the proper heating levels required during rotation. By varying the heater power level, the signal-to-noise ratio of the images could be significantly increased. The voltage was supplied using flat braided copper wire buss bars that were routed along the trailing edge on the upper and lower surfaces. The two independent radial heater zones are depicted in Figure 7. The inboard zone, Zone 2, covered r/R=0.40-0.70 and outboard zone, Zone 1, covered r/R=0.70-1.00. The Zone 1 buss bars were routed at x/c= 0.95 and the Zone 2 buss bars were routed at x/c= 0.89. The buss bar width was 0.30 inches with a height of 0.030 inches. The buss bars were joined in parallel to electrical connectors at the blade root prior to passing through an electrical slip ring mounted in the rotor shaft. Each zone was connected to a remotely controlled 300 voltage direct current (VDC), 5.2 amp power supply in fixed frame on the floor of the RTC.

Two FLIR Systems[TM] SC6701 Strained Layer Superlattice (SLS) cameras were used to acquire simultaneous images of the upper and lower surface of the blade. The cameras have a high sensitivity in the long wave infrared (LWIR) spectral range. Each camera, with a resolution of 640 x 512 pixels, was fitted with an F/2 aperture, 50 mm focal length lens yielding a spatial resolution of 0.055 in/pixel. The lenses were remotely focused using an external belt driven by a piezoelectric rotary actuator. Due to limited depth of field with the F/2 aperture lens, remote focusing was required at each thrust condition to account for the blade elastic deflections. One of the cameras was mounted to the ceiling of the RTC while the other camera was mounted on the floor of the RTC. The camera positions and their corresponding fields of view are shown in Figs. 1-2. The cameras were synced with the rotor RPM using the Rotor Azimuth Synchronization Program (RASP), Ref. 10, to acquire images once per revolution. A series of approximately 575 images per camera were recorded at each thrust condition.

## D.  Fuselage

The fuselage shell was the NASA ROBIN-Mod7 fuselage, an analytically-defined helicopter fuselage model that has been used in numerous prior tests and is meant to represent a generic transport helicopter. The basic dimensions of the fuselage are given in Fig. 8. The rotor shaft angle is -3.5 degrees nose down. The tail cone cap shown aft of FS 105.0 was not installed since the model was mounted on the sting adapter. Greater detail of the fuselage geometry can be found in the publication by Schaeffler et al. (Ref. 11).

## E.  Data Acquisition Systems

The 14x22 facility Data Acquisition System (DAS) was used to acquire the steady-state force and moment data from the rotor and fuselage balances. A detailed description of the 14x22 DAS is provided by Quinto and Orie, Ref. 12. For this test, each data point was taken over a 30 second record length (2300 rotor revolutions) at 50 samples per second. All of the acquired data was passed through a one hertz low-pass filter and 512 analog gain was applied to the rotor and fuselage balances.

# III.   Results

The test results are given in tabular format in Tables 3-11. The data is separated by the test's run number. The table label indicates whether the data is for a natural transition or fixed transition case.

American Institute of Aeronautics and Astronautics

## A.  Hover Performance

The measured rotor hover performance is shown in Fig. 9 in terms of figure of merit as a function of solidity weighted thrust coefficient. The error bars are calculated from the rotor balance calibration accuracies given in Table 1. The natural transition case is represented by the black squares. A maximum figure of merit of 0.79 was measured at $C_T/\sigma = 0.10$. In addition to the natural transition case, data were acquired for three forced transition cases. In each case, transition was forced at x/c=0.05. The three forced transition cases were 1) lower surface only (blue triangles), 2) upper surface only (red circles) and 3) both upper and lower surface (green diamonds).

To calculate the reduction in figure of merit at a given thrust condition, a third-order polynomial was fit to the experimental data. The resulting curves are shown by the solid lines on the left vertical axis in Fig. 10. The dashed curves are the calculated reduction in figure of merit from the natural transition case shown on the right vertical axis. The blue dashed curve, $\Delta L$, is the reduction in figure of merit for fixed transition on only the lower surface. The red dashed curve, $\Delta U$, is the reduction in figure of merit for fixed transition on only the upper surface. The red and blue dashed line, $\Delta U + \Delta L$, represents the summation of the two previous curves. The green curve, $\Delta UL$, is the measured reduction in figure of merit for fixed transition on the upper and lower surfaces combined.

At high thrust, $C_T/\sigma = 0.095$, the figure of merit was decreased by 3.1 counts or 3.7% when fixing transition on the lower surface only. Fixing transition on the upper surface only resulted in a 3.7 count reduction in figure of merit. Fixed transition on the upper and lower surfaces combined resulted in a decrease in figure of merit of 4.9 counts. At low thrust, $C_T/\sigma = 0.040$, the measured reduction in figure of merit was 3.5 and 5.5 counts for the lower and upper surfaces, respectively. Fixed transition on the upper and lower surfaces combined resulted in a 7.1 count decrease in figure of merit.

A brief study of the minimal trip height was conducted on the lower surface from r/R=0.80 to the tip. The forced transition cases were verified by using the IR thermography technique to ensure the blade was in fact turbulent at all radial stations. Originally, a trip height of $h = 1.1$ *mils* was used at x/c=0.05, but the IR images showed transition was not forced. The trip height was increase to $h = 5.0$ *mils* and forced transition was confirmed. The same study was not performed on the upper surface, but it is suspected that the $h = 1.1$ *mils* trip height would have forced transition due to the adverse pressure gradient on the upper surface.

## B.  Transition Locations

The transition locations were measured on the upper and lower surface for each thrust condition. Data were only available outboard of r/R=0.40 where the heater coating was present. The 575 instantaneous images were registered to a common reference to account for global translations and rotations of the model and blades. The registered images were then averaged to a single image to increase the signal-to-noise ratio for each thrust condition. A sample of the infrared thermography images for the upper and lower surfaces at $C_T/\sigma = 0.064$ is shown in Fig. 12. The dark areas represent a turbulent boundary layer or cooler surface temperature a result of the greater heat transfer in the turbulent boundary layer. The transition locations were extracted manually from the averaged image by inspection of the gray scale image. A profile slice through the red line in Fig. 12 is given in Fig. 13. The point along the profile that was extracted as the transition location is the end of the transition band where the flow is fully-turbulent not the start of transition, see Richter and Schulein in Ref. 3 for a detailed description of the data processing technique. The chordwise transition locations were converted to blade coordinates by the appropriate scaling factors.

Comparison of the images of the heated blade to a nonheated blade shows that the nonheated blade has a superior image quality. The nonuniformities in the image are caused by local variations in electrical resistance of the heatable coating. The variation in resistance results in local hot and cold spots on the blade surface. This phenomenon is magnified at the tip where the taper of blade causes the buss bars to be closer together. The shorter buss bar separation distance results in an increased power density of the heater near the tip. The nonuniformities could likely be corrected with background subtraction of a wind-off image or other image processing techniques. At the present time, no formal image processing techniques have been attempted to improve the image quality other than averaging. Despite the challenges with the heater coating, the image quality was sufficient enough to extract the transition locations at numerous thrust conditions without stopping the rotor or changing the rotor RPM to heat the blades. It also allowed for hundreds of images to be acquired at each thrust conditions. For the nonheated blade data acquisition is only possible for several seconds before the ambient and surface temperature of the blade are equal.

In each of the Figs. 15-35, the measured chordwise transition locations are plotted on the vertical axis where the upper surface is a positive chordwise value and the lower surface is given a negative chordwise value. The horizontal axis represents the rotor radius. At the top of each figure, the blade planform is provided to quickly identify the airfoils at each radial station. The area between the two curves is the amount of laminar flow present on the rotor for the

given thrust condition. Small transition wedges are not included in the measured transition locations if they could be explicitly mapped to a local blade surface finish defect. Reliable data is not available aft of x/c=0.90 due to installation of the buss bars for the heaters.

The data is also presented as a function of thrust for three radial stations, r/R=0.65,0.72 and 0.90, in Figs. 36-38. The solid blue curve represents the chordwise transition location on the upper surface and the dashed red line represents the measured transition location on the lower surface. The three radial stations are from sections of the blade, which have different airfoils. The airfoil name and nondimensional shape is given at the bottom of each figure. These data are also summarized in tabular format in Table 3. The three radial stations are representative slices of the blade and quickly show the global transition trends of the rotor. They show that the performance curve can be split into two regions, low and high thrust at a $C_T/\sigma = 0.055$. At this thrust condition, the derivative of the chordwise transition location with respect to thrust is the largest. At low thrust there are moderate amounts ($x_{tr}/c = 0.3 - 0.4$) of laminar flow at the root and extensive amount of laminar flow at the tip $x_{tr}/c = 0.5 - 0.6$. The lower surface exhibits the opposite trend. The transition locations quickly move aft at the root and midspan of the blade sections around $C_T/\sigma = 0.055$. The tip lower surface transition location slowly moves aft up until it is fully laminar at $C_T/\sigma = 0.055$.

## C. Discussion

The measured hover performance for the fixed combined upper and lower transition case is not a summation of the independent fixed upper and lower surface cases. At low thrust on the lower surface, transition is only actually forced on the lower tip region ($r/R > 0.85$) of the blade since the rest of the lower surface is already turbulent. At low thrust on the upper surface, forced transition is only imposed from $r/R = 0.70 - 1.00$. Therefore, the expected result that the profile power increases from a reduction in laminar flow would have a greater impact on hover performance for the fixed upper surface than the lower surface at low thrust is measured. At high thrust, the entire upper surface is turbulent and the lower surface is fully laminar. However, fixed transition on the upper surface only was measured to have a slightly greater impact than fixed transition on only the lower surface. It is possible that the added boundary layer displacement thickness at the leading edge of the upper surface due to the trip dots created turbulent boundary layer separation at the trailing edge. The reduction in figure of merit is then a result of drag due to separation not laminar flow. Although these factors are coupled by the boundary layer thickness rate increase for a turbulent versus laminar boundary layer. For the upper surface inboard airfoils, laminar separation bubbles are likely to form due to the low Reynolds numbers. In this region of the blade, the trip dots could stabilize the boundary layer and prevent the laminar separation bubble from forming thus eliminating the drag due to the separation bubble. Yet, these explanations do not explain why the combined fixed upper and lower surface performance is not a summation of the independently fixed cases.

The competing inboard versus outboard and low versus high thrust effects on the hover performance make it difficult to isolate the effects of transition. By inspection of the measured natural transition locations, an approximate figure of merit curve is estimated for a fully turbulent rotor. The fully turbulent curve is an attempt to isolate the effect of transition on hover performance. The black dashed curve shown in Fig. 11, is estimated by making several assumptions. First, the upper surface is fully turbulent at high thrust ($C_T/\sigma > 0.07$). Therefore, the lower surface forced transition case is assumed to be equal to the fully turbulent case. The next assumption is that at low thrust ($C_T/\sigma < 0.05$), both the upper and lower surface have significant amounts of laminar flow at the rotor tip and the trip dots do not create trailing edge separation. At $C_T/\sigma = 0.03$ the fully turbulent curve is approximated by the summation of the two independent fixed cases. At $C_T/\sigma = 0.05$ the fully turbulent curve is approximated as equal to the upper surface only fixed data. Obviously, the assumptions above are approximations and do not represent measured experimental data. The only true unaltered data is the natural transition case. In conjunction with measured locations, the natural transition case should be used for comparisons to predictions.

A more detailed trip dot height study is required to fully understand the fixed transition data. The study must account for Reynolds number effects, airfoil changes and pressure gradients; therefore, detailed IR thermography images are required of the leading- and trailing-edge regions of the full rotor radius. At the leading edge, the IR images should document the boundary layer state and any separation bubbles. At the trailing edge, the IR images should document the extent of trailing-edge separation. Higher spatial resolution measurements than were acquired during this test would be required to make these conclusions. In addition, the electrical buss bar placement at the trailing edge prevented measurements of trailing-edge separation during this test.

## IV.  Conclusions

A Mach-scaled rotor test was completed with the rotor performance and boundary layer transition locations measured as a function of rotor thrust. An improvement to the IR thermography technique to measure boundary layer transition on a rotor was presented. The use of a paintable heater and new LWIR cameras made it feasible to acquire large amounts of boundary layer transition data.

The data presented is intended to be a preliminary data set used for the development and implementation of boundary layer transition tools in CFD codes. The measured transition locations showed extensive amounts, $x/c >$ 0.90, of laminar flow on the lower surface at moderate to high thrust ($C_T/\sigma > 0.068$) conditions for the full blade radius. The upper surface showed large amounts, $x/c > 0.50$, of laminar flow at the blade tip for low thrust ($C_T/\sigma <$ 0.045). A peak figure of merit of 0.79 was measured for the natural transition case at ($C_T/\sigma = 0.10$). The test data highlights the importance of measuring the boundary layer state and its effect on the measured hover performance. At high thrust, $C_T/\sigma = 0.090$, the figure of merit was decreased by the 3.1 counts or 3.7% when fixing transition only on the lower surface. The figure of merit was further reduced when fixing transition on the upper surface. The fixed upper surface data is likely influenced by trailing-edge separation; therefore, a more detailed experimental study is required to understand the fixed transition data cases. The measured natural transition locations on the upper and lower surface for the entire rotor radius are required to understand the measured hover performance. Blindly adding trip dots to force transition could yield unexpected results not representative of a fully turbulent rotor.

The government is currently designing and fabricating a new blade set with identical planform and airfoils with embedded heaters for the purpose of generating a validation data set. The new embedded heaters are designed to maximize the temperature uniformity and allow for measurements near the trailing-edge and tip regions of the blade.

## V.  Acknowledgments

## References

[1]Boatwright, D., "Three-Dimensional Measurements of the Velocity in the Near FLow Field of a Full-Scale Hovering Rotor," *AD-781-547*, 1974.

[2]Martin, P., "Martin Thesis," *University of Maryland*, May 2001.

[3]Richter, K. and Schulein, E., "Boundary Layer Transition Measurements on Hovering Helicopter Rotors by Infrared Thermography," *American Helicopter Society 70th Annual Forum*, Montreal, Quebec, Canada, May 20-22 2014.

[4]Richter, K., Schulein, E., Ewers, B., Raddatz, J., and Klein, A., "Boundary Layer Transition Characteristics of a Full-Scale Helicopter Rotor in Hover," *American Helicopter Society 72nd Annual Forum*, West Palm Beach, FL, May 17-19 2016.

[5]Tanner, W. and Yaggy, P., "Experimental Boundary Layer Study on Hovering Rotors," *Journal of the American Helicopter Society*, 1966.

[6]Wadock, A., Yamauchi, G., and Driver, D., "Skin Friction Measurements of a Hovering Full-Scale Tilt Rotor," *Journal of the American Helicopter Society*, 1999.

[7]Richter, K. and Schulein, E., "Boundary-layer transition measurements on hovering helicopter rotors by infrared thermography," *Experimental in Fluids*, 2014.

[8]Murrill, R., "Operation and Maintenance Manual for the General Rotor Model System," *SER-50986, NAS1-12674*, May 1977.

[9]Wong, O. D., Noonan, K. W., Watkins, A. N., Jenkins, L. N., , and Yao, C. S., "Non-Intrusive Measurements of a Four-Bladed Rotor in Hover  A First Look," *American Helicopter Society Aeromechanics Specialists Conference*, San Francisco, CA, January 2010.

[10]Fleming, G. A., "Rotor Azimuth Synchronization Program (RASP) User's Guide, Version 1.3," *NASA Langley Research Center*, 2008.

[11]Schaeffler, N., Allan, B., Lienard, C., and Le Pape, A., "Progress Towards Fuselage Drag Reduction via Active Flow Control: A Combined CFD and Experimental Effort," *36th European Rotorcraft Forum*, Paris, France, Sept 7-9 2010.

[12]Quinto, P. F. and Orie, N. M., "Langley 14- by 22-Foot Subsonic Tunnel Test Engineers Data Acquisition and Reduction Manual," *NASA TM- 4563*, Langley Research Center, June 2014.
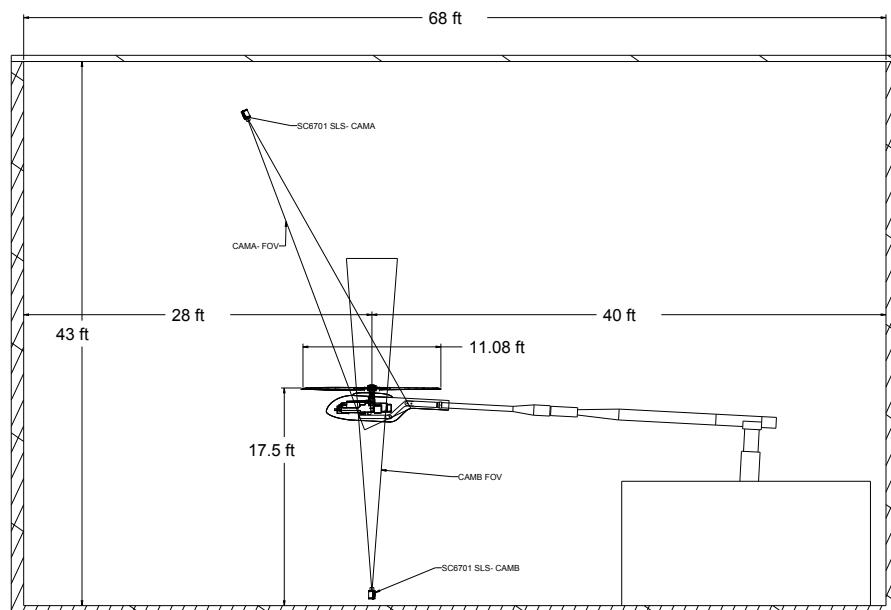
American Institute of Aeronautics and Astronautics

**Figure 1. Schematic of the experimental test setup in the RTC- Side View.**
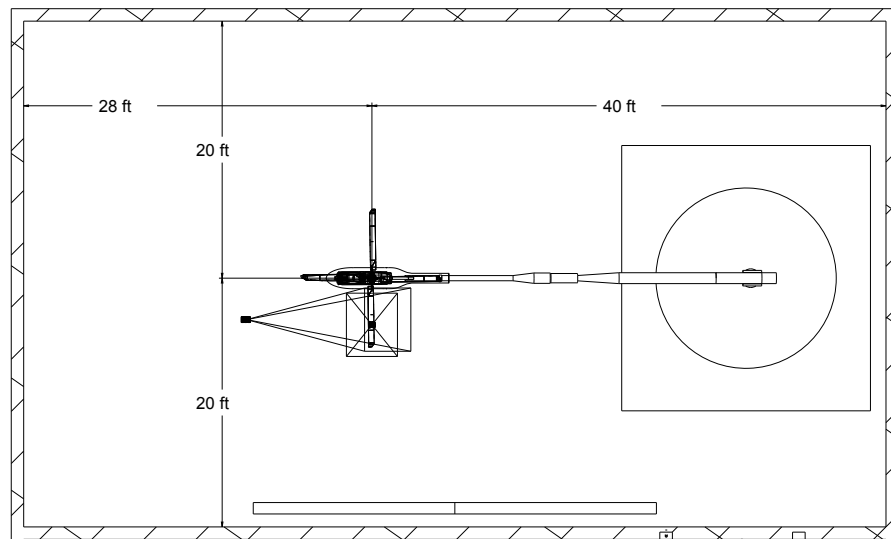


**Figure 2. Schematic of the experimental test setup in the RTC- Top View.**

American Institute of Aeronautics and Astronautics
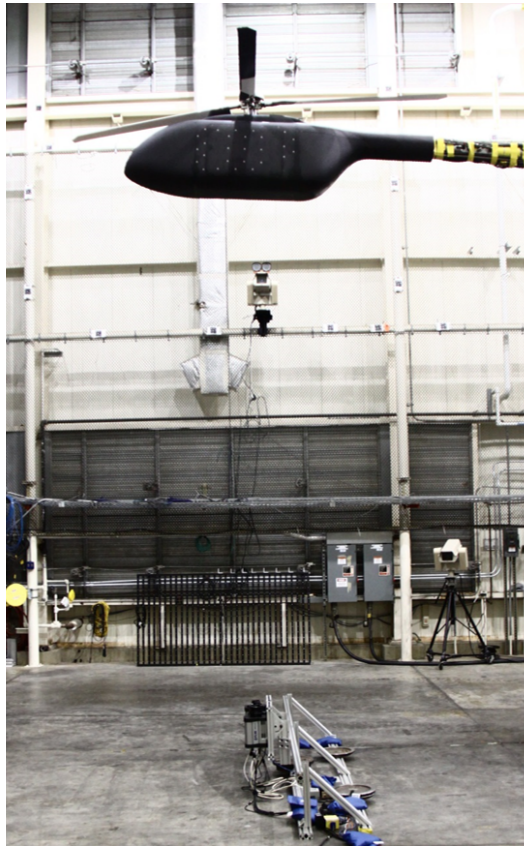
**Figure 3.  Picture of the experimental test setup.**
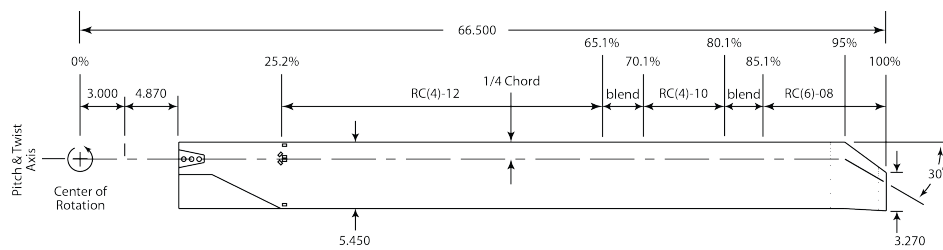


**Figure 4.  PSP Blade Planform, inches.**
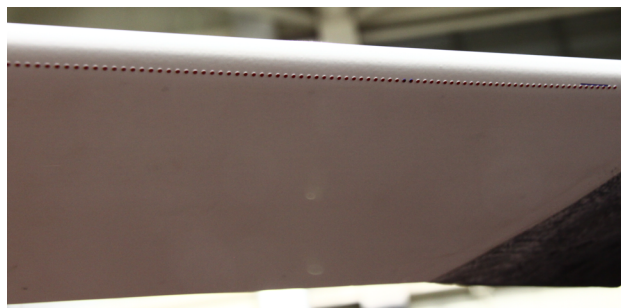


**Figure 5.  Blade Root Lower Surface Trip Dots, h=9.9 mil.**

American Institute of Aeronautics and Astronautics
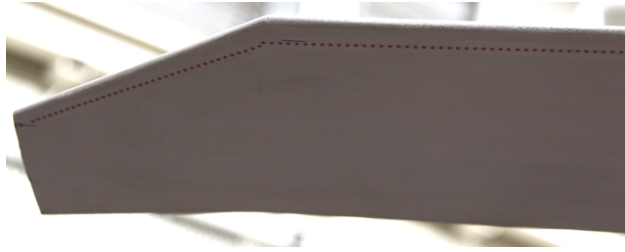
**Figure 6.  Blade Tip Lower Surface Trip Dots, h=5.0 mil.**
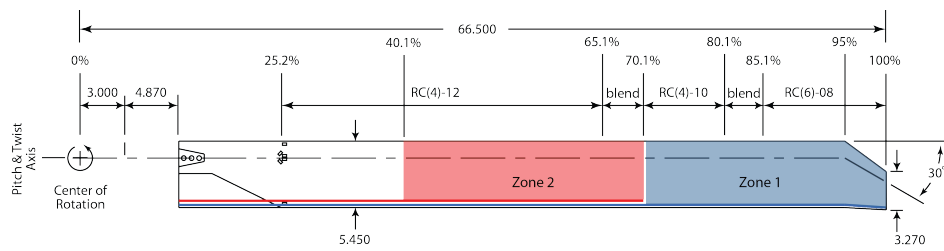


**Figure 7.  Blade Heater Zone Definitions, inches.**
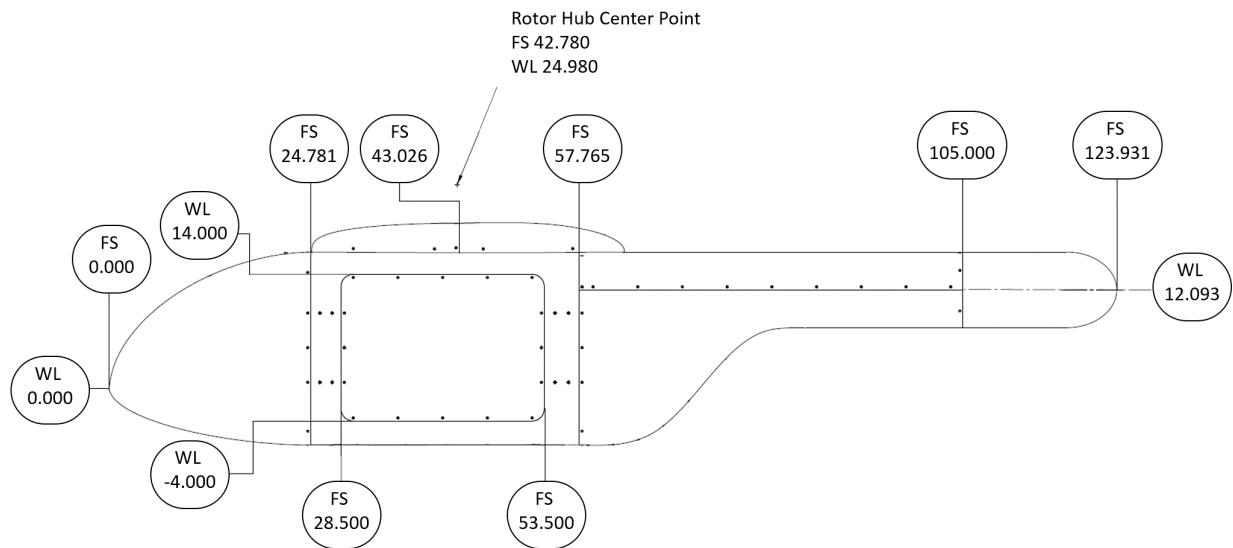


**Figure 8.  Basic Dimensions of Robin-Mod7 Fuselage.**

American Institute of Aeronautics and Astronautics
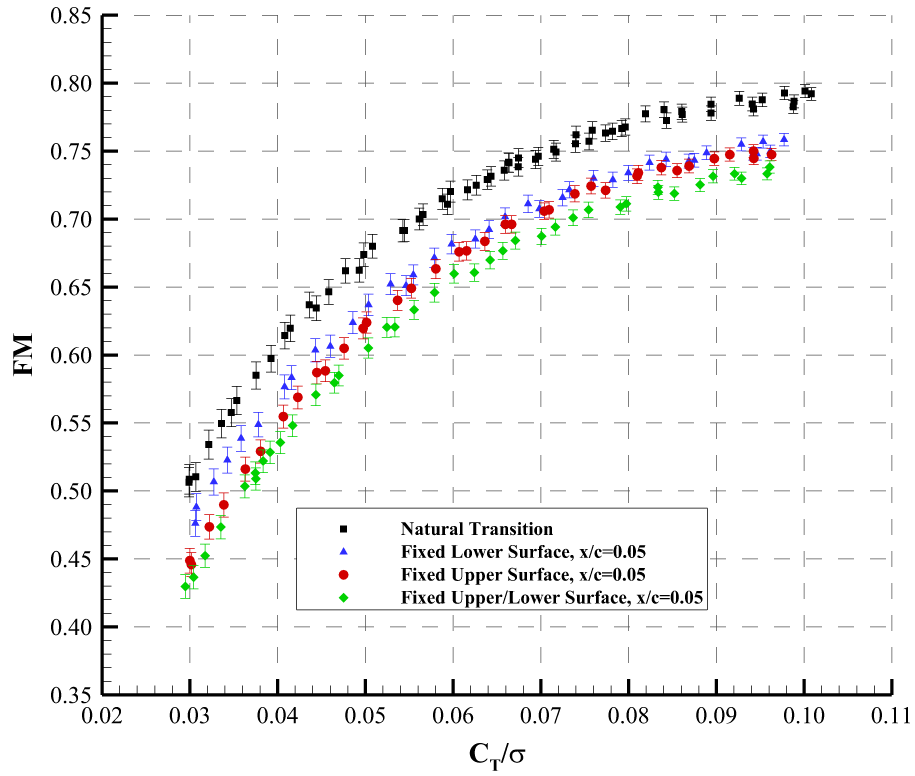
**Figure 9. Measured PSP Blade Hover Performance.**
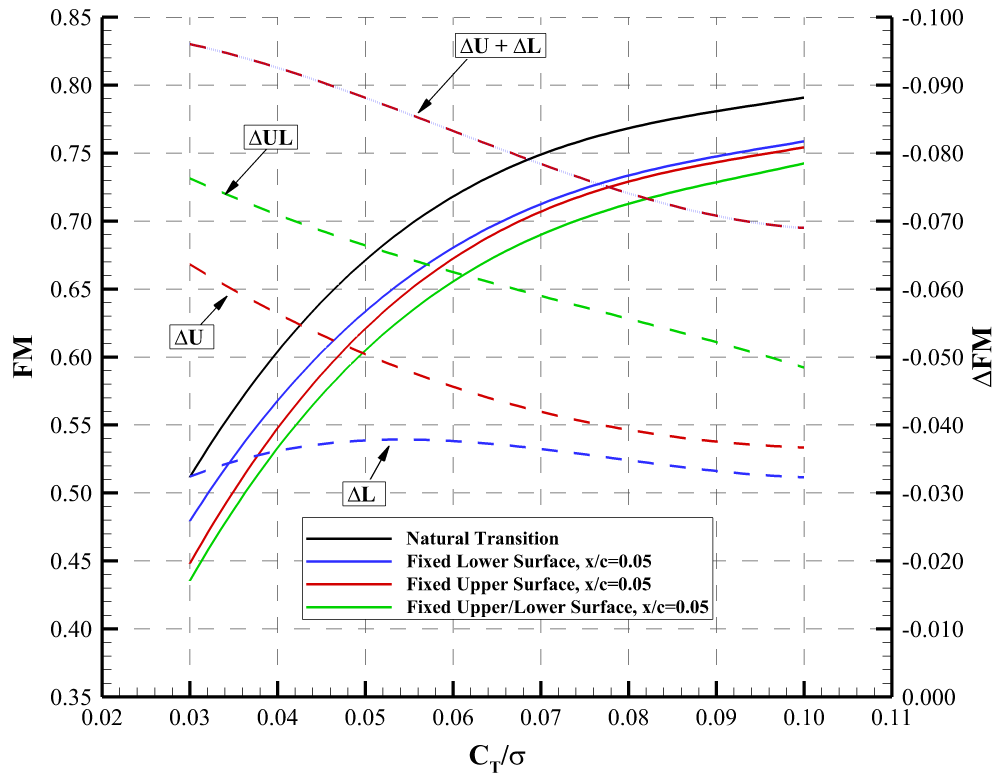


**Figure 10. Effect of Forced Transition on Hover Performance.**

American Institute of Aeronautics and Astronautics
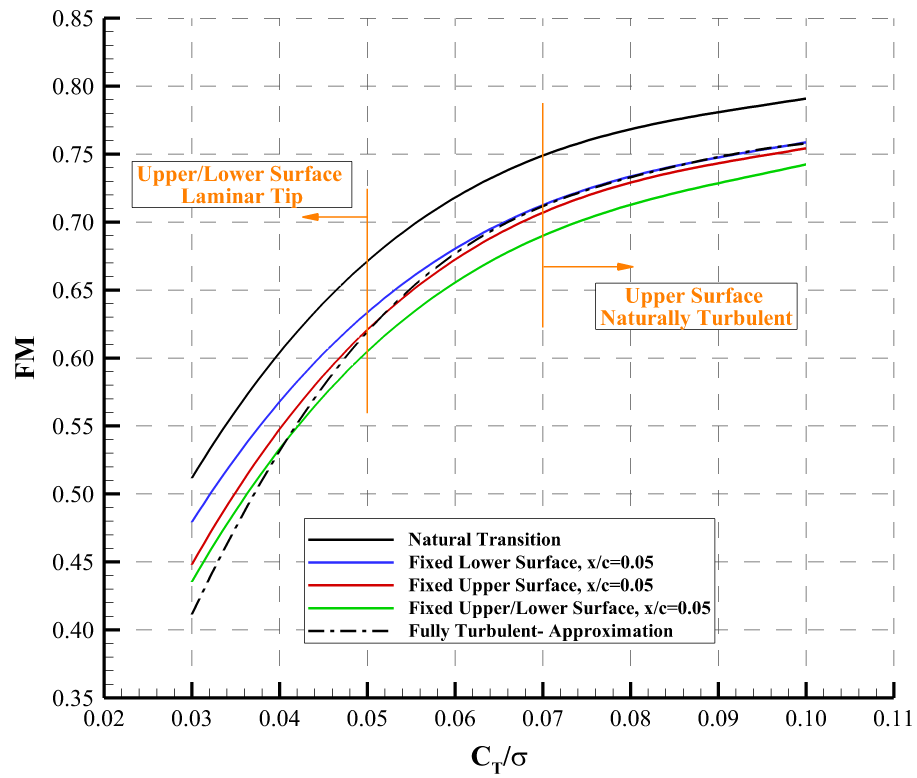
**Figure 11. Approximated Fully Turbulent Figure of Merit.**

American Institute of Aeronautics and Astronautics
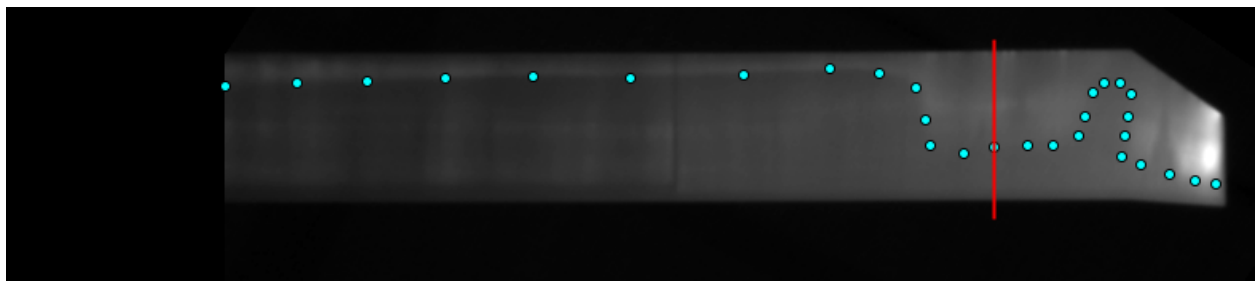
**Figure 12. Sample infrared thermography image of lower surface , $C_T/\sigma = 0.035$.**
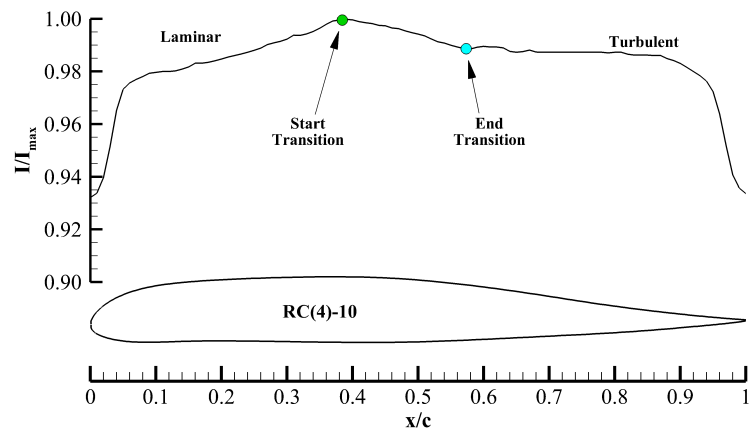


**Figure 13. Line profile of image intensity and transition locations.**
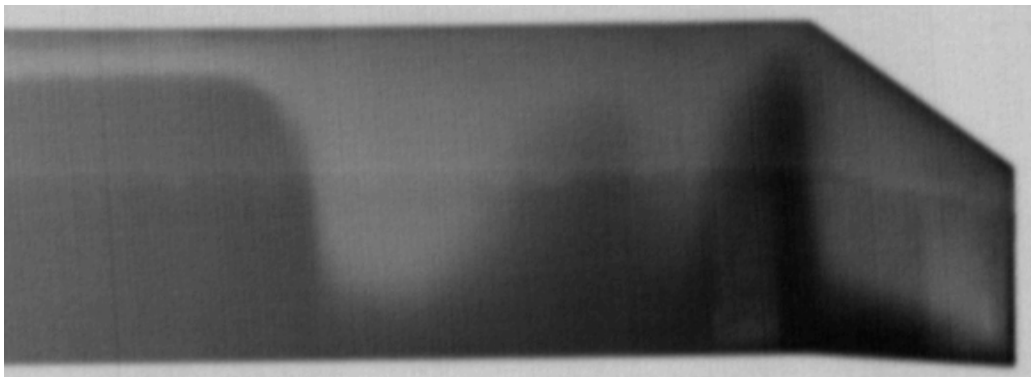


**Figure 14. Sample infrared thermography image of without heater coating, lower surface $C_T/\sigma \approx 0.035$.**

American Institute of Aeronautics and Astronautics

**Figure 15. Measured Transition Locations,** $C_T/\sigma = 0.030$.
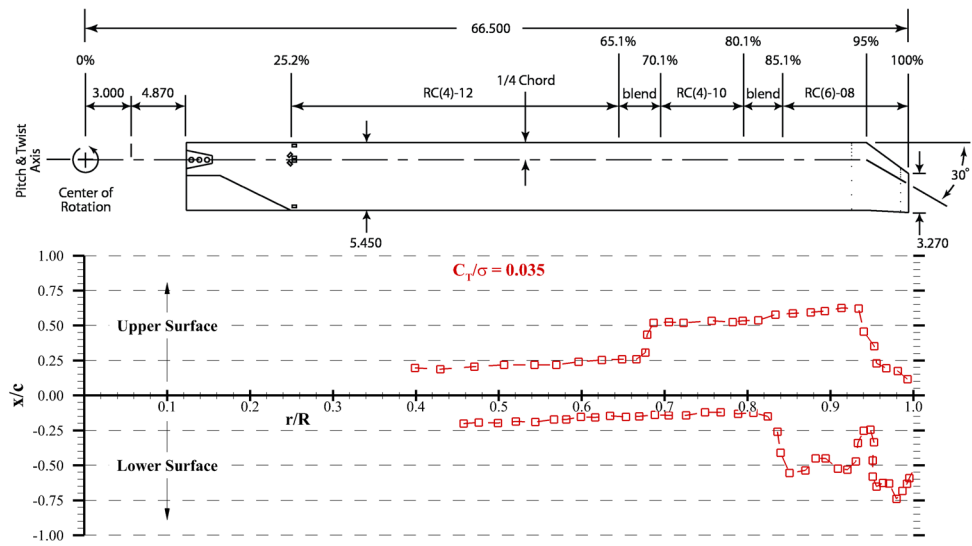


**Figure 16. Measured Transition Locations,** $C_T/\sigma = 0.035$.

**Figure 17. Measured Transition Locations,** $C_T/\sigma = 0.040$.
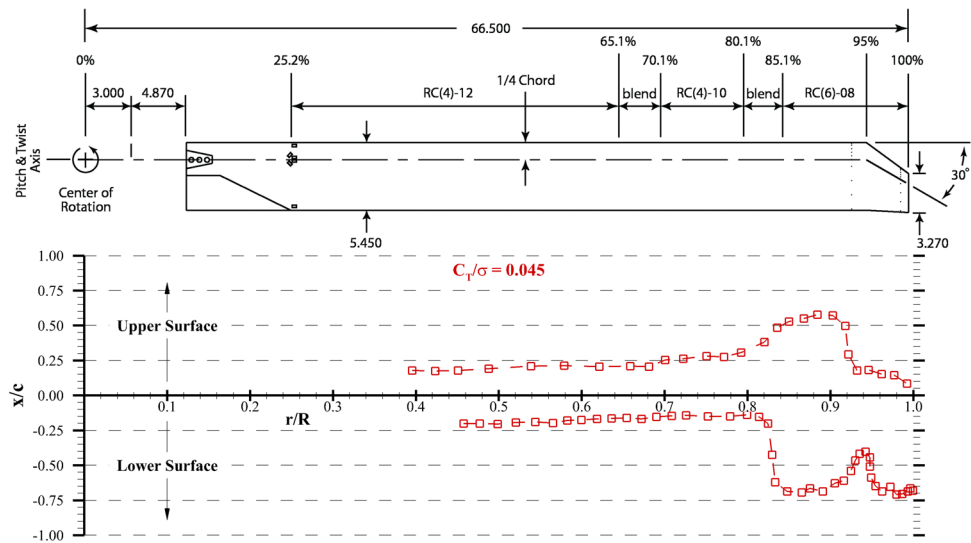


**Figure 18. Measured Transition Locations,** $C_T/\sigma = 0.045$.

American Institute of Aeronautics and Astronautics

**Figure 19. Measured Transition Locations,** $C_T/\sigma = 0.050$.
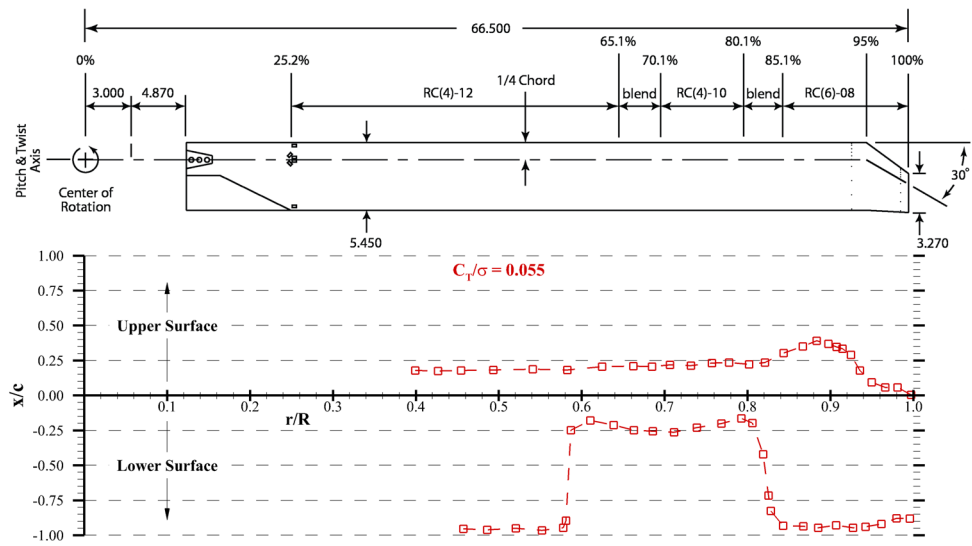


**Figure 20. Measured Transition Locations,** $C_T/\sigma = 0.055$.

American Institute of Aeronautics and Astronautics

**Figure 21. Measured Transition Locations,** $C_T/\sigma = 0.060$.



**Figure 22. Measured Transition Locations,** $C_T/\sigma = 0.062$.

American Institute of Aeronautics and Astronautics

**Figure 23. Measured Transition Locations, $C_T/\sigma = 0.064$.**
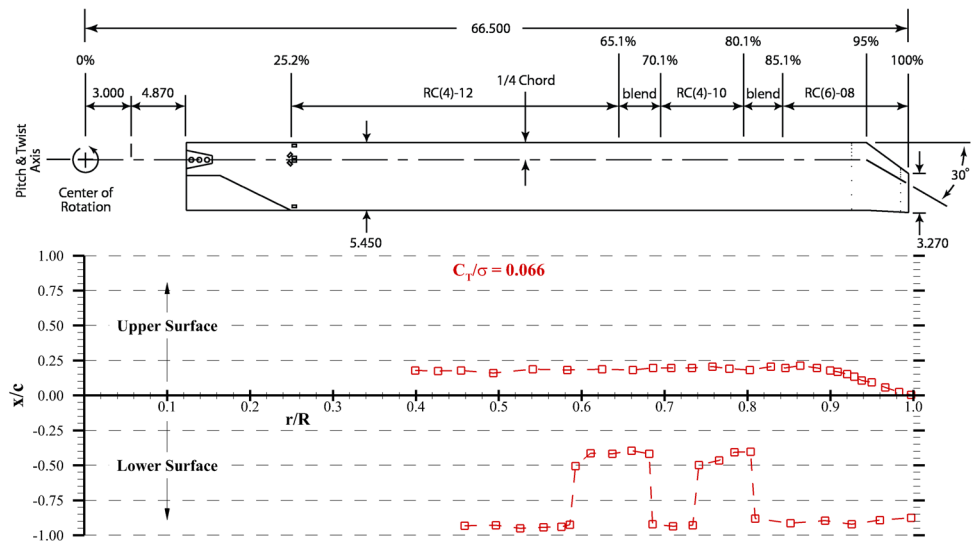


**Figure 24. Measured Transition Locations, $C_T/\sigma = 0.066$.**

**Figure 25. Measured Transition Locations, $C_T/\sigma = 0.068$.**
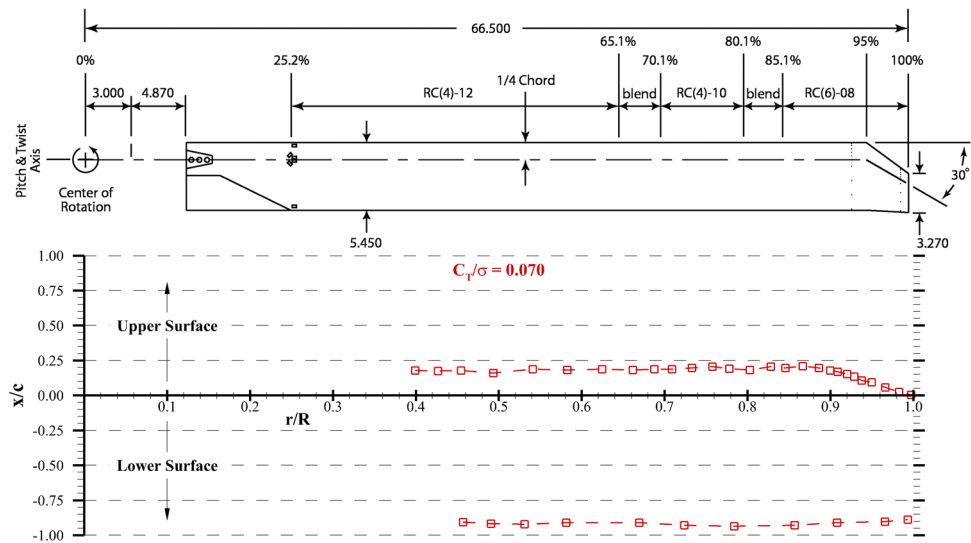


**Figure 26. Measured Transition Locations, $C_T/\sigma = 0.070$.**

American Institute of Aeronautics and Astronautics
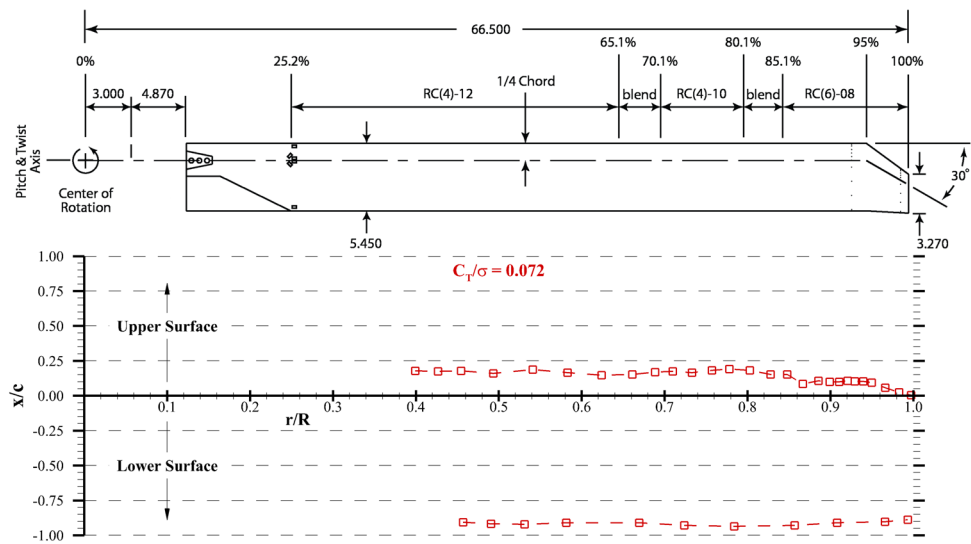
**Figure 27. Measured Transition Locations,** $C_T/\sigma = 0.072$.



**Figure 28. Measured Transition Locations,** $C_T/\sigma = 0.074$.

American Institute of Aeronautics and Astronautics
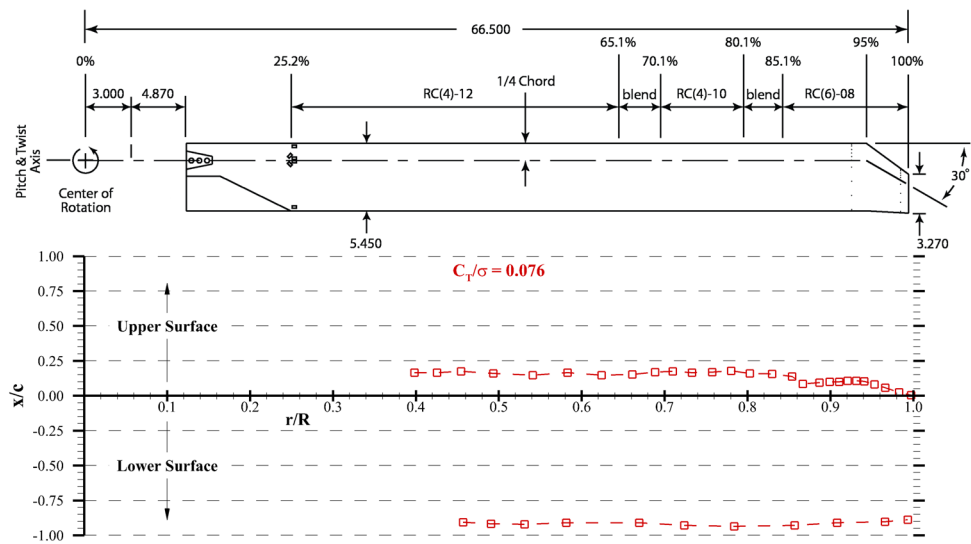
**Figure 29. Measured Transition Locations,** $C_T/\sigma = 0.076$.
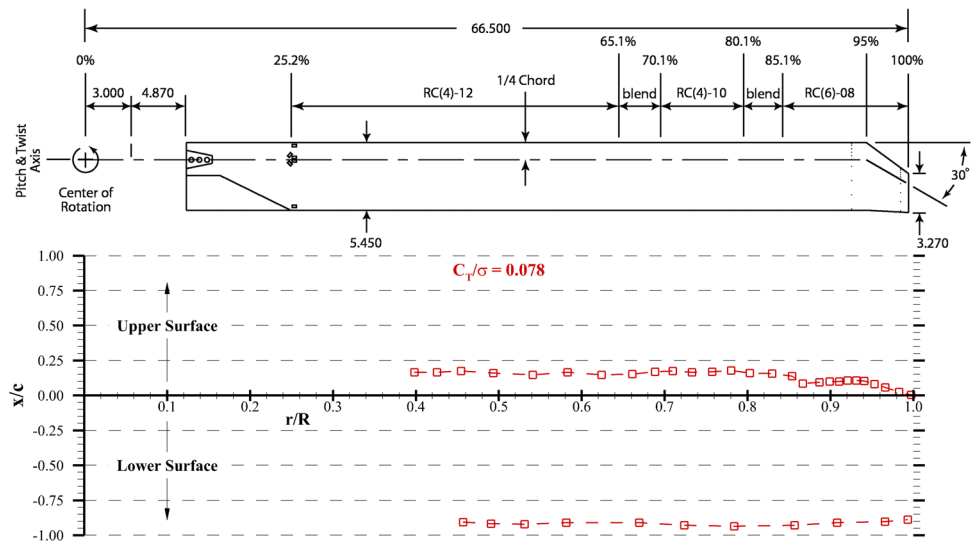


**Figure 30. Measured Transition Locations,** $C_T/\sigma = 0.078$.
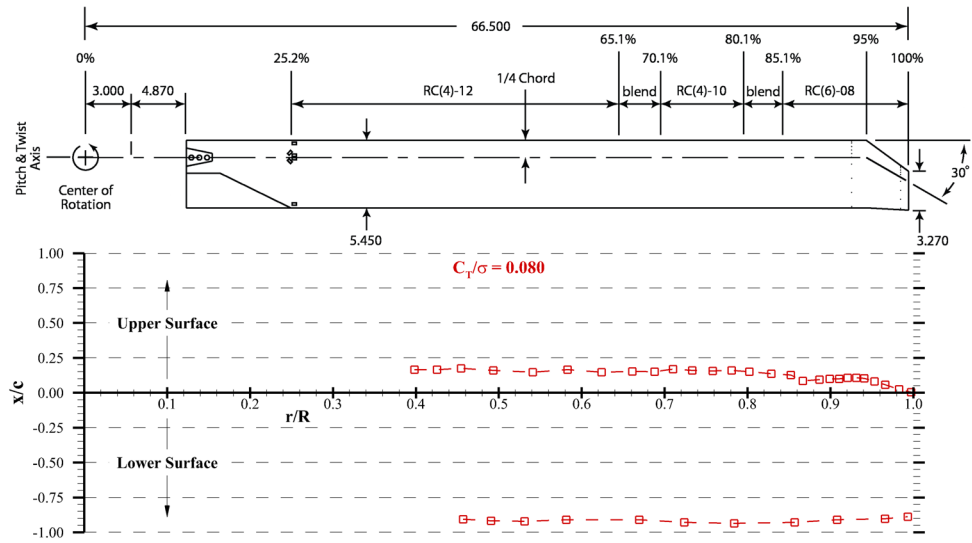
**Figure 31. Measured Transition Locations, $C_T/\sigma = 0.080$.**
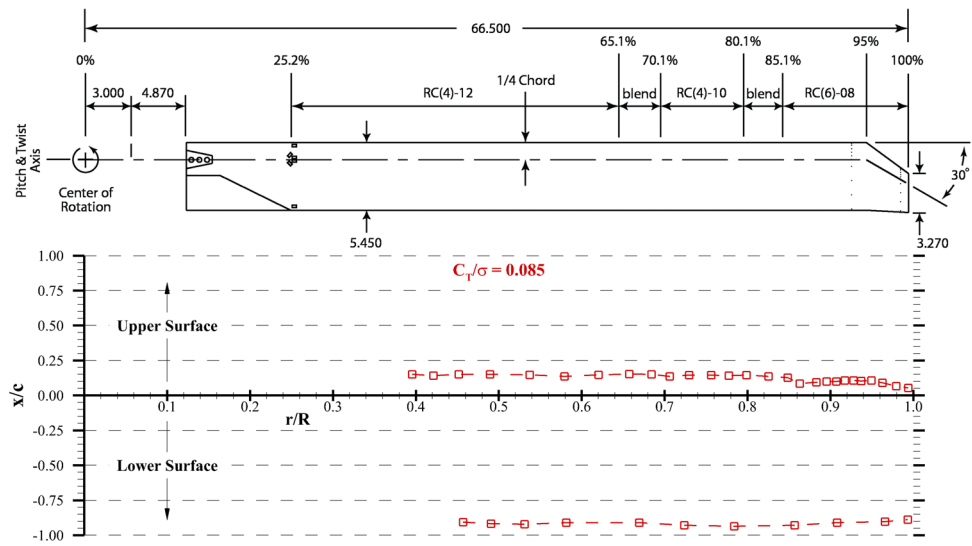


**Figure 32. Measured Transition Locations, $C_T/\sigma = 0.085$.**

American Institute of Aeronautics and Astronautics
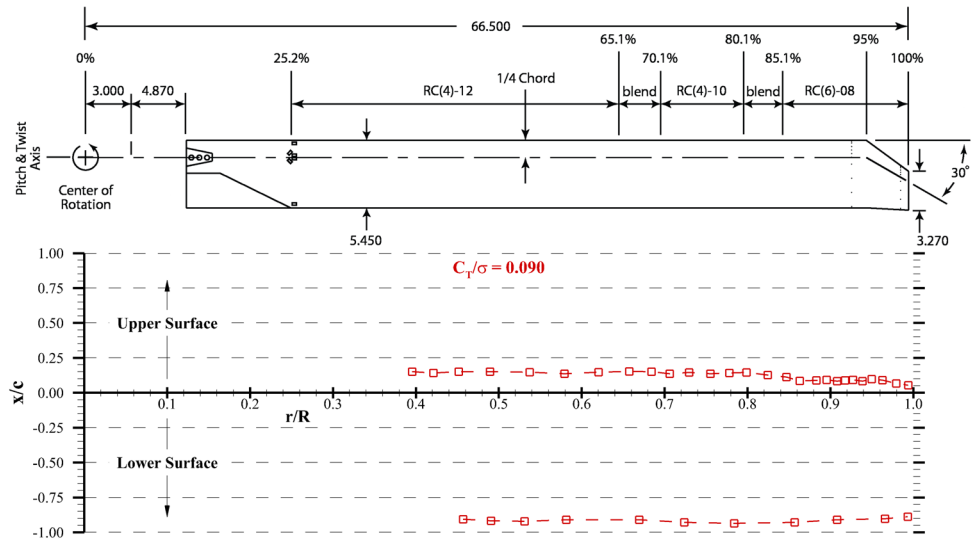
**Figure 33. Measured Transition Locations,** $C_T/\sigma = 0.090$.
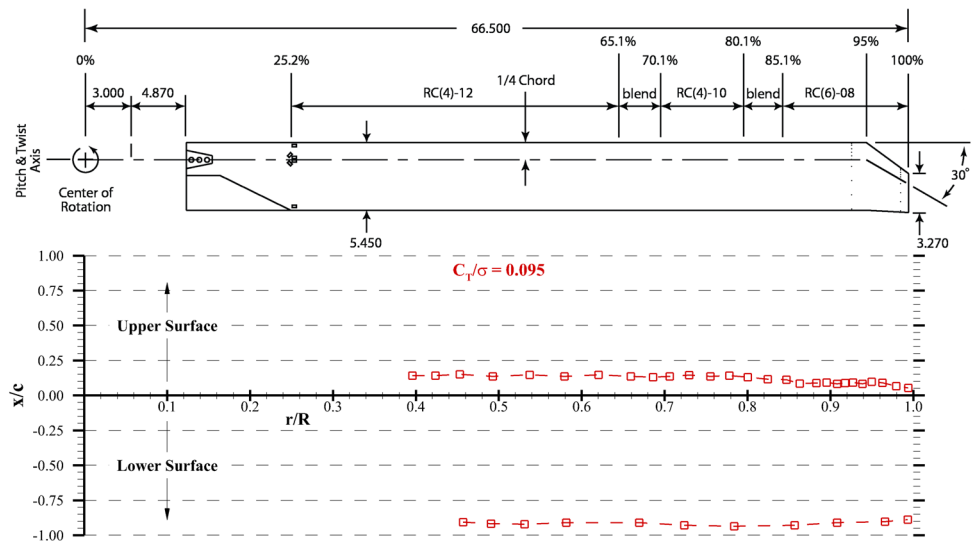


**Figure 34. Measured Transition Locations,** $C_T/\sigma = 0.095$.

American Institute of Aeronautics and Astronautics
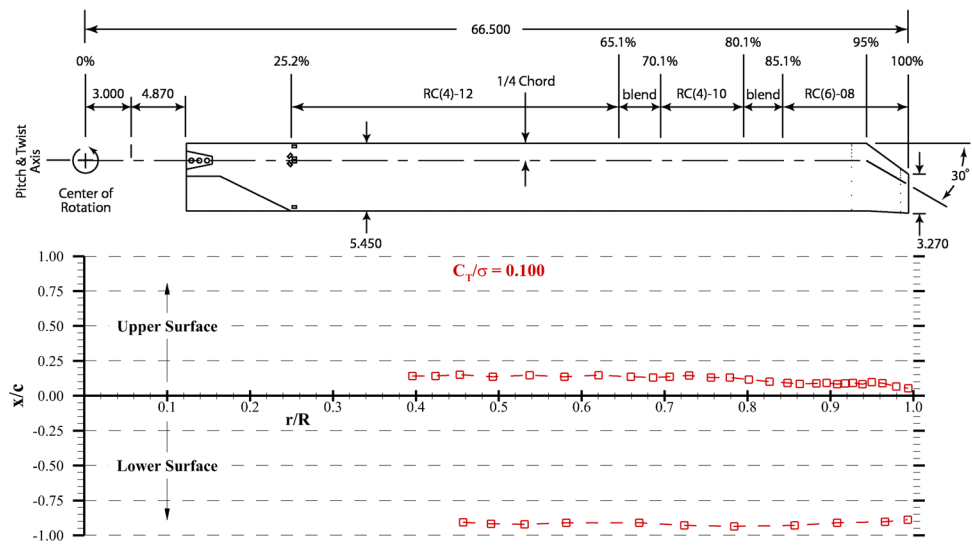
**Figure 35. Measured Transition Locations, $C_T/\sigma = 0.100$.**
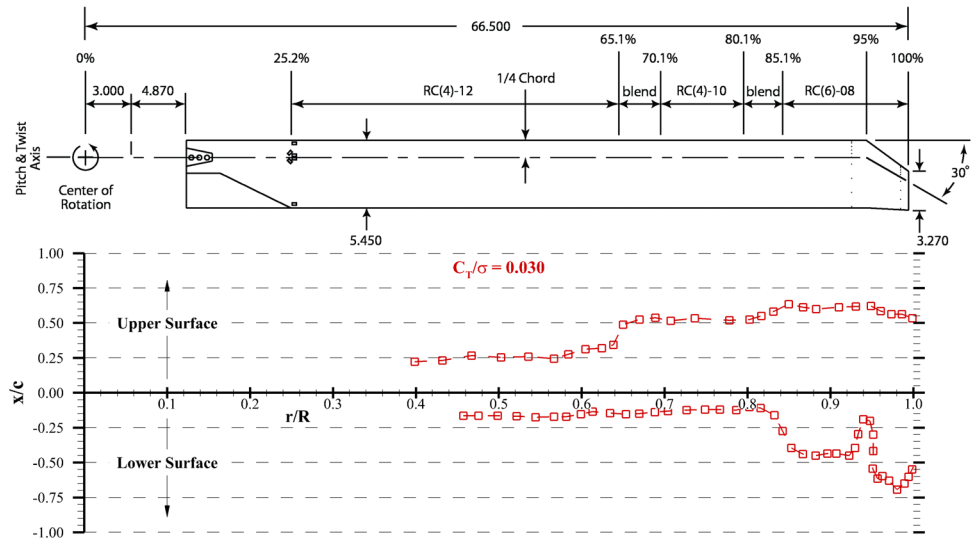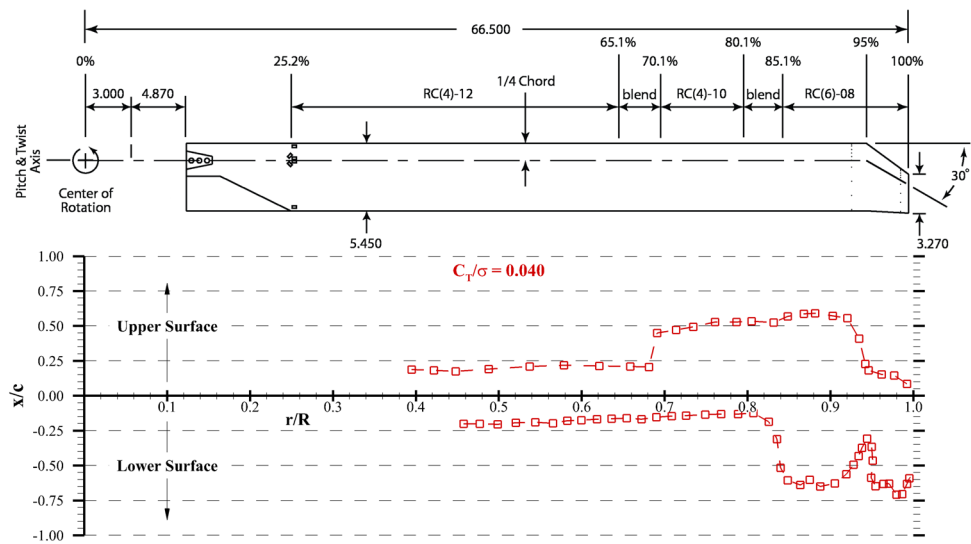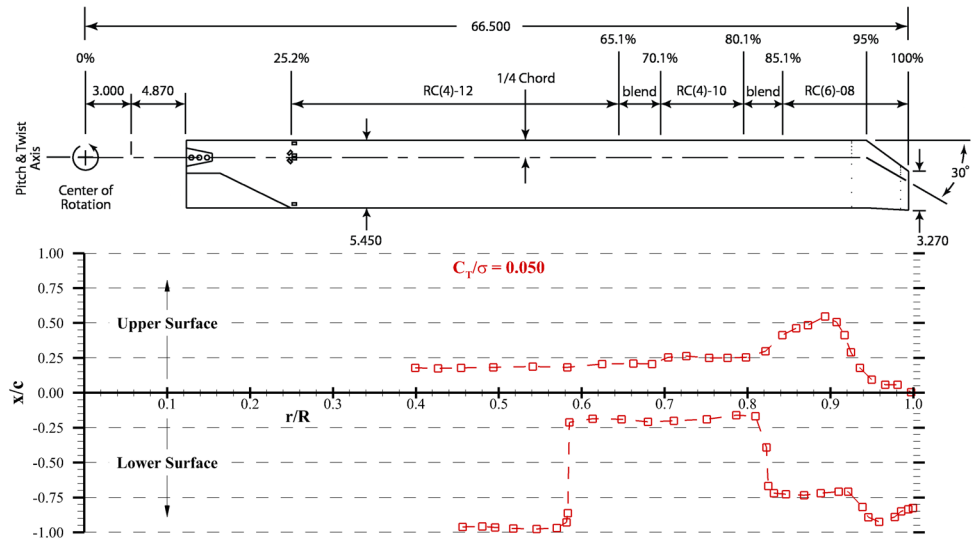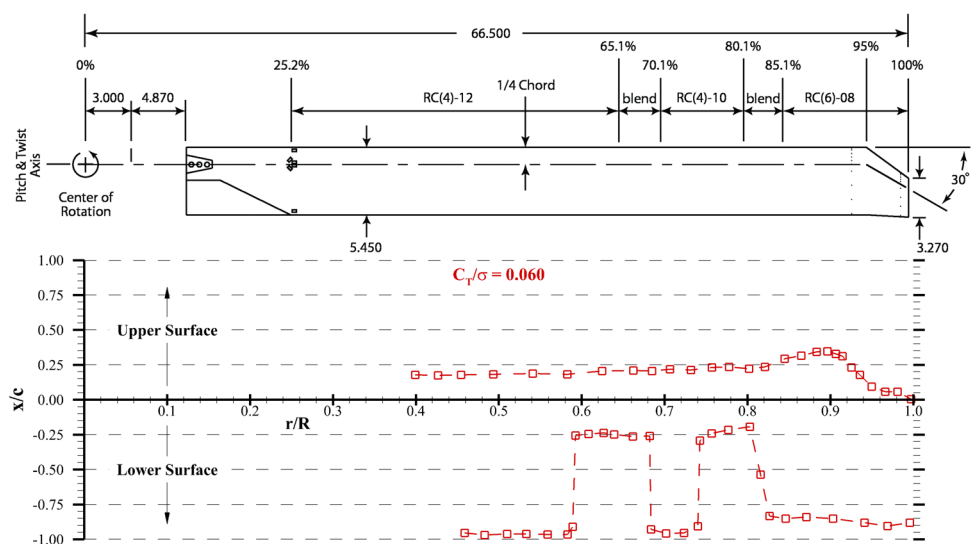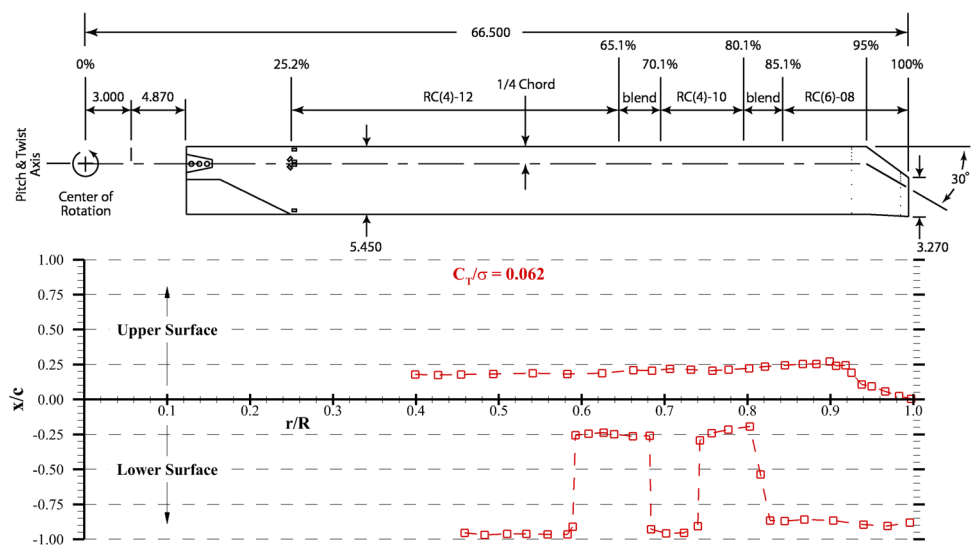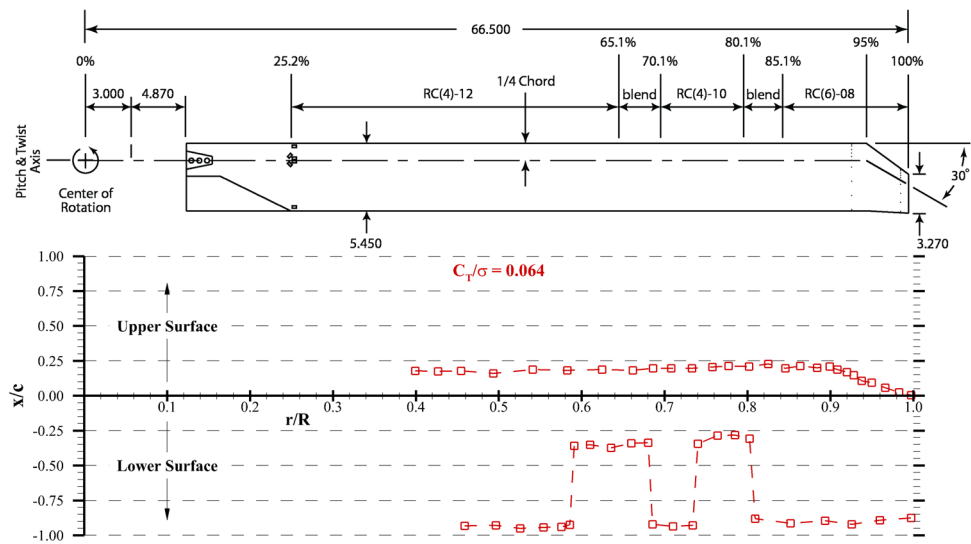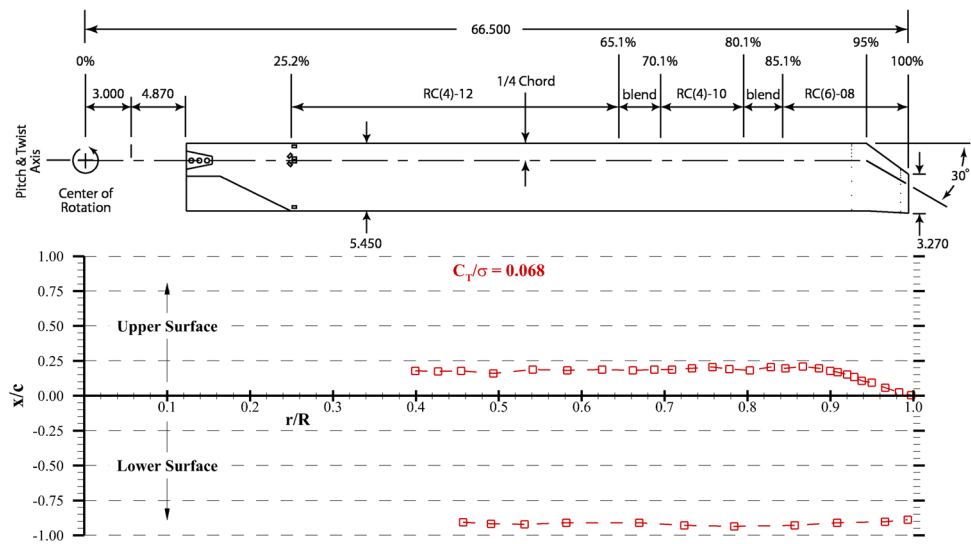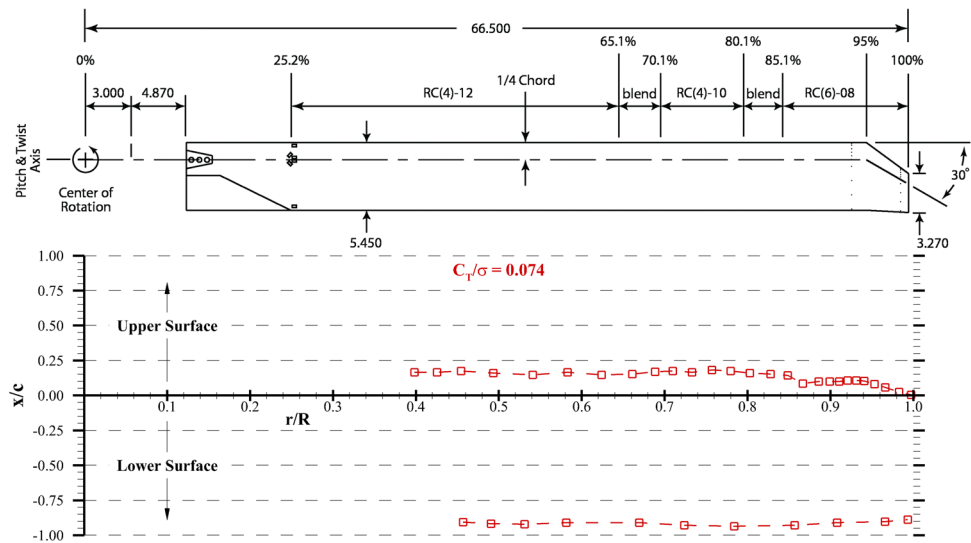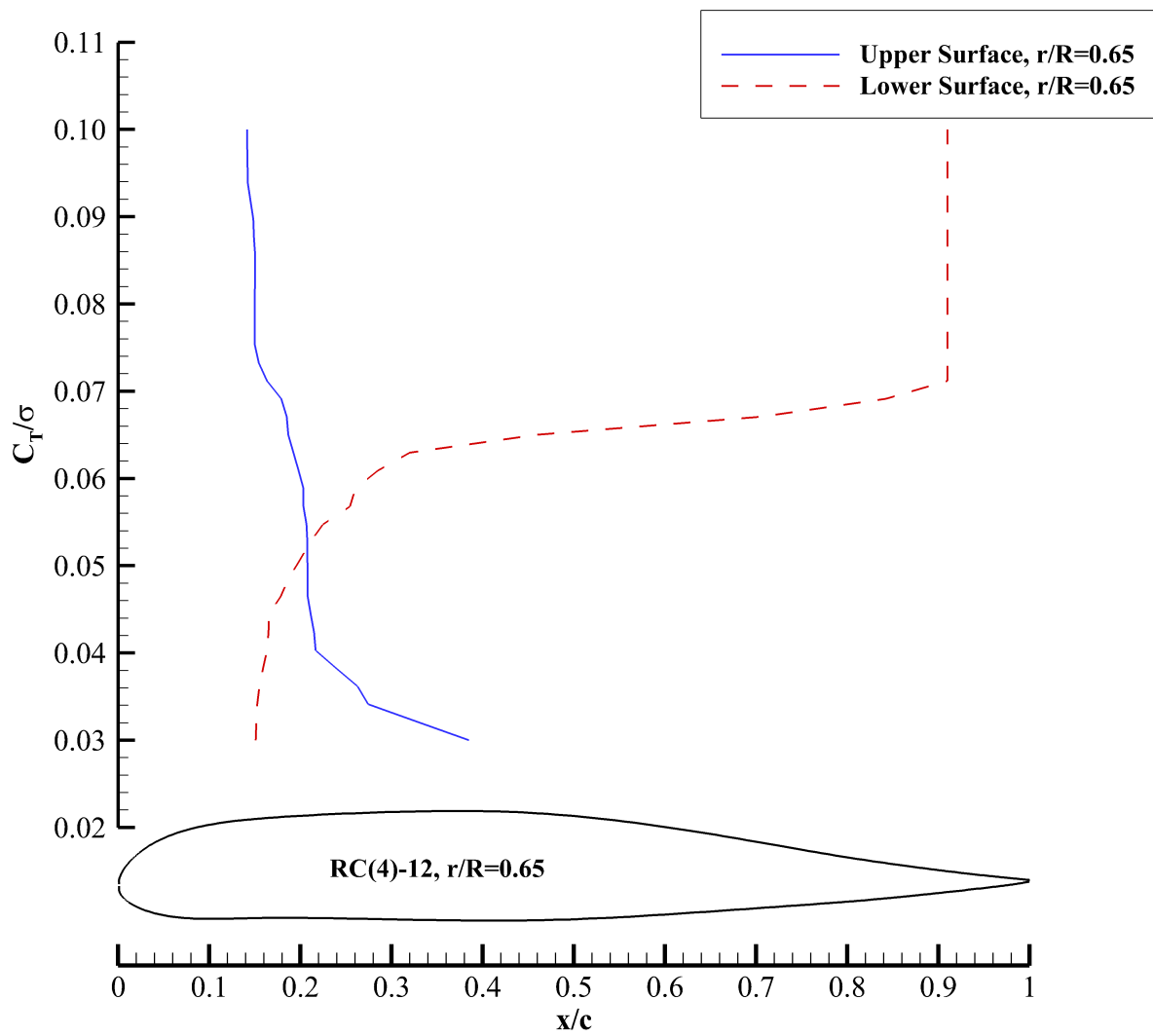
**Figure 36. Measured Transition Locations, r/R=0.65.**
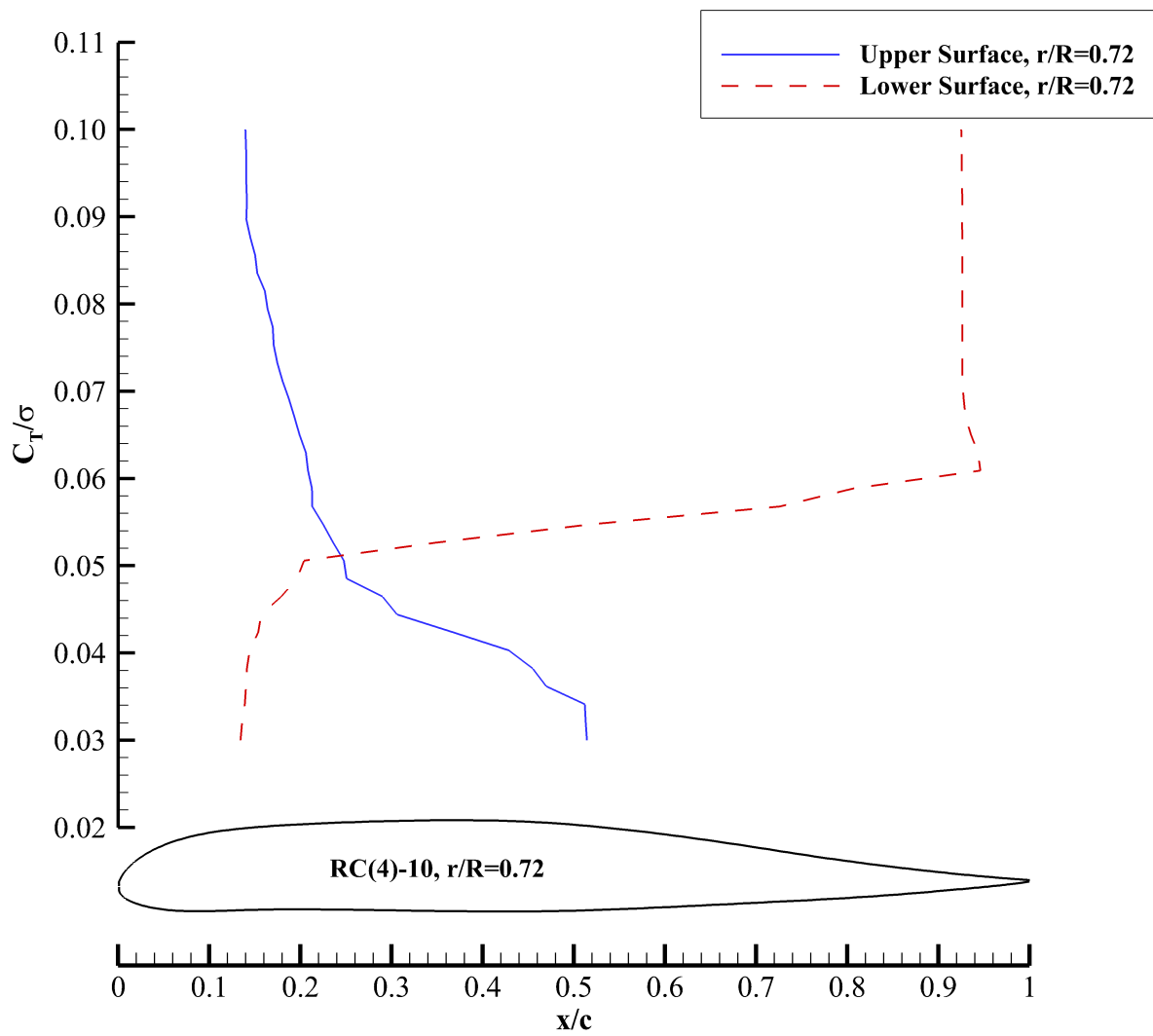
**Figure 37. Measured Transition Locations, r/R=0.72.**

American Institute of Aeronautics and Astronautics
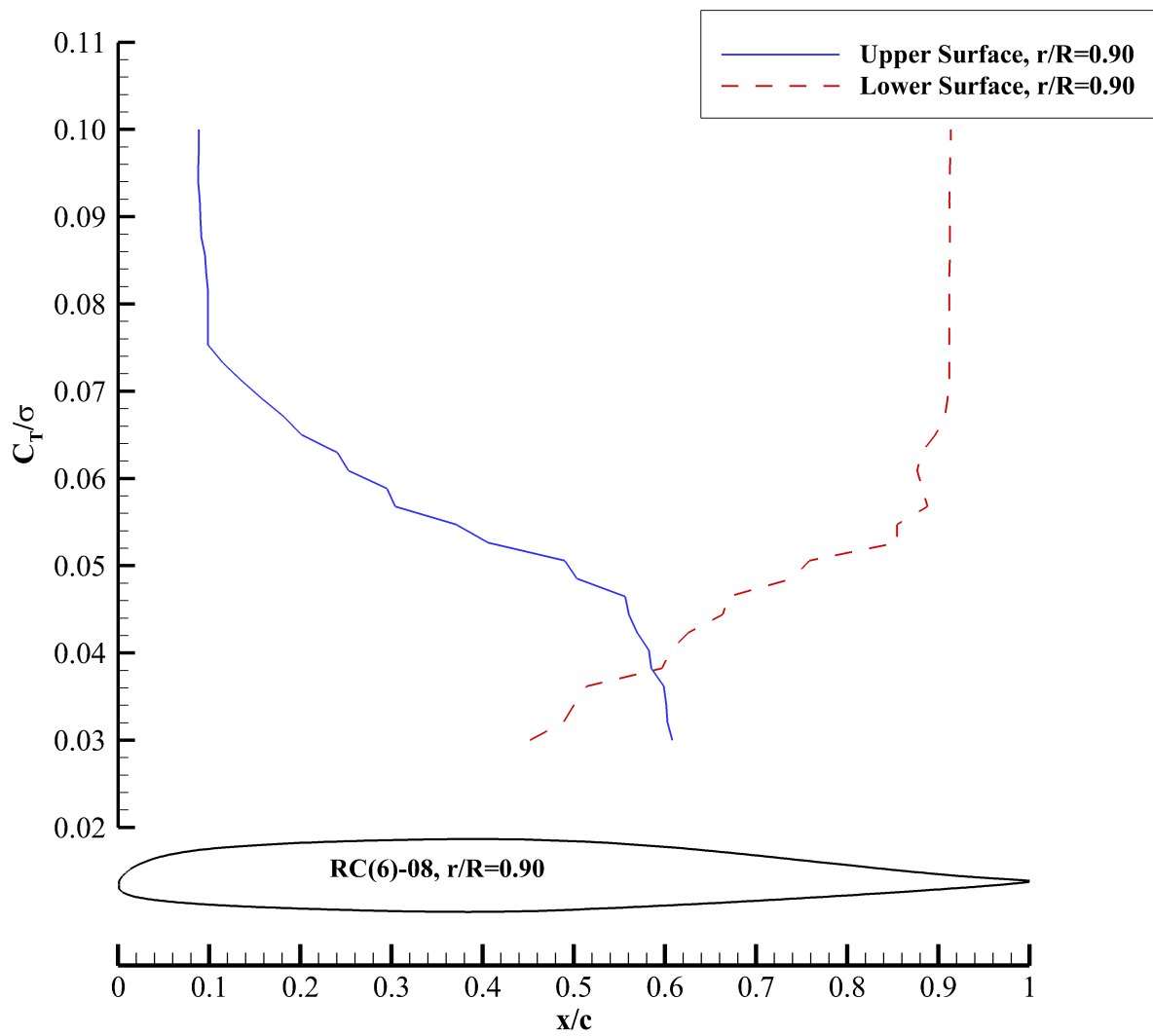
**Figure 38.  Measured Transition Locations, r/R=0.90.**

American Institute of Aeronautics and Astronautics

**Table 3. Test 622 Run 118- Natural Transition.**

| Point | $C_T/\sigma$ | $C_P$ | FM | $\theta_{0.75}$ | $M_{tip}$ | TA | PA | $\rho$ | $x_{tr,l-0.65}$ | $x_{tr,l-0.72}$ | $x_{tr,l-0.90}$ | $x_{tr,u-0.65}$ | $x_{tr,u-0.72}$ | $x_{tr,u-0.90}$ |
|---|---|---|---|---|---|---|---|---|---|---|---|---|---|---|
| - | - | - | - | deg | - | degF | psf | $slug/ft^3$ | - | - | - | - | - | - |
| 788 | 0.030 | 0.000240 | 0.506 | 6.27 | 0.585 | 82.40 | 2120.00 | 0.00226 | 0.15 | 0.13 | 0.45 | 0.39 | 0.51 | 0.61 |
| 789 | 0.035 | 0.000272 | 0.558 | 6.91 | 0.585 | 82.60 | 2120.00 | 0.00226 | 0.15 | 0.14 | 0.51 | 0.26 | 0.47 | 0.60 |
| 790 | 0.039 | 0.000306 | 0.597 | 7.47 | 0.585 | 82.70 | 2120.00 | 0.00225 | 0.16 | 0.14 | 0.61 | 0.22 | 0.43 | 0.58 |
| 791 | 0.044 | 0.000346 | 0.634 | 8.08 | 0.585 | 82.80 | 2120.00 | 0.00225 | 0.17 | 0.16 | 0.66 | 0.21 | 0.31 | 0.56 |
| 792 | 0.049 | 0.000388 | 0.662 | 8.67 | 0.585 | 83.00 | 2120.00 | 0.00225 | 0.20 | 0.20 | 0.76 | 0.21 | 0.25 | 0.49 |
| 793 | 0.055 | 0.000431 | 0.692 | 9.20 | 0.584 | 83.30 | 2120.00 | 0.00225 | 0.22 | 0.52 | 0.85 | 0.21 | 0.23 | 0.37 |
| 794 | 0.059 | 0.000478 | 0.711 | 9.73 | 0.584 | 83.50 | 2120.00 | 0.00225 | 0.28 | 0.95 | 0.88 | 0.20 | 0.21 | 0.25 |
| 795 | 0.062 | 0.000498 | 0.721 | 9.97 | 0.584 | 83.70 | 2120.00 | 0.00225 | 0.32 | 0.94 | 0.88 | 0.19 | 0.21 | 0.24 |
| 796 | 0.064 | 0.000520 | 0.729 | 10.20 | 0.584 | 83.90 | 2120.00 | 0.00225 | 0.46 | 0.94 | 0.90 | 0.19 | 0.20 | 0.20 |
| 797 | 0.066 | 0.000539 | 0.736 | 10.40 | 0.584 | 84.00 | 2120.00 | 0.00225 | 0.71 | 0.93 | 0.91 | 0.19 | 0.19 | 0.18 |
| 798 | 0.067 | 0.000557 | 0.738 | 10.60 | 0.584 | 84.10 | 2120.00 | 0.00225 | 0.84 | 0.93 | 0.91 | 0.18 | 0.19 | 0.16 |
| 799 | 0.070 | 0.000579 | 0.746 | 10.80 | 0.584 | 84.40 | 2120.00 | 0.00225 | 0.91 | 0.93 | 0.91 | 0.16 | 0.18 | 0.14 |
| 800 | 0.072 | 0.000602 | 0.749 | 11.00 | 0.584 | 84.50 | 2120.00 | 0.00225 | 0.91 | 0.93 | 0.91 | 0.15 | 0.17 | 0.12 |
| 801 | 0.074 | 0.000625 | 0.755 | 11.20 | 0.584 | 84.60 | 2120.00 | 0.00225 | 0.91 | 0.93 | 0.91 | 0.15 | 0.17 | 0.10 |
| 802 | 0.075 | 0.000643 | 0.757 | 11.40 | 0.584 | 84.80 | 2120.00 | 0.00225 | 0.91 | 0.93 | 0.91 | 0.15 | 0.17 | 0.10 |
| 803 | 0.077 | 0.000662 | 0.763 | 11.60 | 0.583 | 85.00 | 2120.00 | 0.00225 | 0.91 | 0.93 | 0.91 | 0.15 | 0.16 | 0.10 |
| 804 | 0.079 | 0.000683 | 0.767 | 11.80 | 0.583 | 85.10 | 2120.00 | 0.00224 | 0.91 | 0.93 | 0.91 | 0.15 | 0.16 | 0.10 |
| 805 | 0.084 | 0.000744 | 0.772 | 12.30 | 0.583 | 85.30 | 2120.00 | 0.00224 | 0.91 | 0.93 | 0.91 | 0.15 | 0.15 | 0.10 |
| 806 | 0.089 | 0.000807 | 0.778 | 12.80 | 0.583 | 85.50 | 2120.00 | 0.00224 | 0.91 | 0.93 | 0.91 | 0.15 | 0.14 | 0.09 |
| 807 | 0.094 | 0.000870 | 0.781 | 13.30 | 0.583 | 85.60 | 2120.00 | 0.00224 | 0.91 | 0.93 | 0.91 | 0.14 | 0.14 | 0.09 |
| 808 | 0.099 | 0.000931 | 0.782 | 13.70 | 0.583 | 85.90 | 2120.00 | 0.00224 | 0.91 | 0.93 | 0.91 | 0.14 | 0.14 | 0.09 |
| 809 | 0.056 | 0.000446 | 0.700 | 9.35 | 0.583 | 85.80 | 2120.00 | 0.00224 | 0.22 | 0.52 | 0.85 | 0.21 | 0.23 | 0.37 |

American Institute of Aeronautics and Astronautics

**Table 4. Test 622 Run 147- Natural Transition.**

| Point | $C_T/\sigma$ | $C_P$ | FM | $\theta_{0.75}$ | $M_{tip}$ | TA | PA | $\rho$ |
|---|---|---|---|---|---|---|---|---|
| - | - | - | - | deg | - | degF | psf | $slug/ft^3$ |
| 1166 | 0.031 | 0.000247 | 0.510 | 6.65 | 0.585 | 81.75 | 2119.04 | 0.00226 |
| 1167 | 0.038 | 0.000292 | 0.585 | 7.50 | 0.585 | 82.24 | 2119.04 | 0.00226 |
| 1168 | 0.046 | 0.000356 | 0.646 | 8.46 | 0.585 | 82.55 | 2119.04 | 0.00226 |
| 1169 | 0.054 | 0.000429 | 0.691 | 9.35 | 0.584 | 82.81 | 2119.04 | 0.00226 |
| 1170 | 0.063 | 0.000508 | 0.725 | 10.20 | 0.585 | 83.03 | 2119.04 | 0.00226 |
| 1171 | 0.069 | 0.000577 | 0.744 | 10.92 | 0.584 | 83.25 | 2119.04 | 0.00226 |
| 1172 | 0.078 | 0.000671 | 0.764 | 11.80 | 0.584 | 83.46 | 2118.83 | 0.00225 |
| 1173 | 0.086 | 0.000761 | 0.779 | 12.56 | 0.584 | 83.89 | 2118.83 | 0.00225 |
| 1174 | 0.094 | 0.000864 | 0.785 | 13.38 | 0.584 | 84.16 | 2118.83 | 0.00225 |
| 1175 | 0.099 | 0.000928 | 0.787 | 13.84 | 0.584 | 84.50 | 2118.83 | 0.00225 |
| 1176 | 0.095 | 0.000876 | 0.788 | 13.45 | 0.584 | 84.66 | 2118.62 | 0.00225 |
| 1177 | 0.086 | 0.000764 | 0.777 | 12.60 | 0.583 | 84.81 | 2118.62 | 0.00225 |
| 1178 | 0.080 | 0.000687 | 0.768 | 11.96 | 0.583 | 84.88 | 2118.62 | 0.00225 |
| 1179 | 0.071 | 0.000597 | 0.751 | 11.14 | 0.583 | 84.93 | 2118.62 | 0.00225 |
| 1180 | 0.064 | 0.000524 | 0.731 | 10.38 | 0.583 | 84.93 | 2118.62 | 0.00225 |
| 1181 | 0.057 | 0.000449 | 0.703 | 9.57 | 0.584 | 84.88 | 2118.83 | 0.00225 |
| 1182 | 0.048 | 0.000370 | 0.662 | 8.61 | 0.584 | 84.88 | 2118.83 | 0.00225 |
| 1183 | 0.041 | 0.000315 | 0.614 | 7.81 | 0.584 | 84.84 | 2118.83 | 0.00225 |
| 1184 | 0.032 | 0.000253 | 0.534 | 6.77 | 0.584 | 84.78 | 2118.83 | 0.00225 |

**Table 5. Test 622 Run 148- Natural Transition.**

| Point | $C_T/\sigma$ | $C_P$ | FM | $\theta_{0.75}$ | $M_{tip}$ | TA | PA | $\rho$ |
|---|---|---|---|---|---|---|---|---|
| - | - | - | - | deg | - | degF | psf | $slug/ft^3$ |
| 1185 | 0.034 | 0.000263 | 0.550 | 6.93 | 0.584 | 84.71 | 2118.83 | 0.00225 |
| 1186 | 0.041 | 0.000320 | 0.620 | 7.89 | 0.584 | 84.66 | 2118.83 | 0.00225 |
| 1187 | 0.050 | 0.000387 | 0.674 | 8.83 | 0.584 | 84.71 | 2118.83 | 0.00225 |
| 1188 | 0.059 | 0.000468 | 0.715 | 9.74 | 0.584 | 84.75 | 2118.83 | 0.00225 |
| 1189 | 0.066 | 0.000541 | 0.742 | 10.56 | 0.584 | 84.86 | 2118.83 | 0.00225 |
| 1190 | 0.066 | 0.000542 | 0.741 | 10.57 | 0.584 | 84.91 | 2118.83 | 0.00225 |
| 1191 | 0.074 | 0.000620 | 0.762 | 11.33 | 0.584 | 85.09 | 2118.83 | 0.00225 |
| 1192 | 0.082 | 0.000708 | 0.777 | 12.11 | 0.584 | 85.24 | 2119.04 | 0.00225 |
| 1193 | 0.089 | 0.000798 | 0.784 | 12.87 | 0.583 | 85.41 | 2119.04 | 0.00224 |
| 1194 | 0.098 | 0.000905 | 0.793 | 13.66 | 0.583 | 85.66 | 2119.04 | 0.00224 |
| 1195 | 0.100 | 0.000937 | 0.794 | 13.90 | 0.583 | 85.93 | 2119.04 | 0.00224 |
| 1196 | 0.101 | 0.000949 | 0.792 | 14.00 | 0.583 | 86.10 | 2119.24 | 0.00224 |
| 1197 | 0.093 | 0.000839 | 0.789 | 13.16 | 0.583 | 86.25 | 2119.24 | 0.00224 |
| 1198 | 0.084 | 0.000733 | 0.781 | 12.31 | 0.583 | 86.30 | 2119.24 | 0.00224 |
| 1199 | 0.076 | 0.000641 | 0.765 | 11.49 | 0.583 | 86.34 | 2119.24 | 0.00224 |
| 1200 | 0.067 | 0.000552 | 0.745 | 10.66 | 0.583 | 86.33 | 2119.24 | 0.00224 |
| 1201 | 0.060 | 0.000476 | 0.720 | 9.86 | 0.583 | 86.26 | 2119.45 | 0.00224 |
| 1202 | 0.051 | 0.000396 | 0.680 | 8.93 | 0.583 | 86.20 | 2119.45 | 0.00224 |
| 1203 | 0.044 | 0.000336 | 0.637 | 8.12 | 0.583 | 86.13 | 2119.45 | 0.00224 |
| 1204 | 0.035 | 0.000275 | 0.567 | 7.16 | 0.583 | 86.06 | 2119.45 | 0.00224 |
| 1205 | 0.030 | 0.000239 | 0.508 | 6.43 | 0.583 | 85.97 | 2119.45 | 0.00224 |

American Institute of Aeronautics and Astronautics

**Table 6. Test 622 Run 153- Forced Transition x/c=0.05 Lower Surface.**

| Point | $C_T/\sigma$ | $C_P$ | FM | $\theta_{0.75}$ | $M_{tip}$ | TA | PA | $\rho$ |
|---|---|---|---|---|---|---|---|---|
| - | - | - | - | $deg$ | - | $degF$ | $psf$ | $slug/ft^3$ |
| 1256 | 0.031 | 0.000264 | 0.476 | 6.64 | 0.585 | 81.50 | 2124.88 | 0.00227 |
| 1257 | 0.038 | 0.000315 | 0.549 | 7.55 | 0.585 | 81.88 | 2124.88 | 0.00227 |
| 1258 | 0.046 | 0.000382 | 0.606 | 8.53 | 0.585 | 82.15 | 2124.88 | 0.00226 |
| 1259 | 0.055 | 0.000461 | 0.651 | 9.48 | 0.585 | 82.39 | 2124.88 | 0.00226 |
| 1260 | 0.063 | 0.000536 | 0.685 | 10.32 | 0.585 | 82.59 | 2124.88 | 0.00226 |
| 1261 | 0.070 | 0.000612 | 0.707 | 11.10 | 0.584 | 82.76 | 2125.09 | 0.00226 |
| 1262 | 0.078 | 0.000704 | 0.729 | 11.93 | 0.585 | 82.99 | 2124.88 | 0.00226 |
| 1263 | 0.087 | 0.000809 | 0.743 | 12.84 | 0.584 | 83.23 | 2124.88 | 0.00226 |
| 1264 | 0.094 | 0.000908 | 0.748 | 13.62 | 0.584 | 83.50 | 2124.88 | 0.00226 |
| 1265 | 0.095 | 0.000913 | 0.748 | 13.67 | 0.584 | 83.78 | 2124.88 | 0.00226 |
| 1266 | 0.096 | 0.000934 | 0.750 | 13.81 | 0.584 | 83.98 | 2124.88 | 0.00226 |
| 1267 | 0.087 | 0.000817 | 0.743 | 12.88 | 0.584 | 84.20 | 2124.88 | 0.00226 |
| 1268 | 0.080 | 0.000723 | 0.734 | 12.12 | 0.584 | 84.29 | 2124.88 | 0.00226 |
| 1269 | 0.072 | 0.000640 | 0.716 | 11.33 | 0.584 | 84.34 | 2124.88 | 0.00226 |
| 1270 | 0.064 | 0.000550 | 0.692 | 10.44 | 0.584 | 84.36 | 2124.88 | 0.00226 |
| 1271 | 0.055 | 0.000465 | 0.659 | 9.54 | 0.584 | 84.32 | 2124.88 | 0.00226 |
| 1272 | 0.049 | 0.000403 | 0.624 | 8.78 | 0.584 | 84.27 | 2124.88 | 0.00226 |
| 1273 | 0.041 | 0.000336 | 0.577 | 7.85 | 0.584 | 84.24 | 2124.88 | 0.00226 |
| 1274 | 0.033 | 0.000274 | 0.507 | 6.86 | 0.584 | 84.15 | 2124.68 | 0.00226 |

American Institute of Aeronautics and Astronautics

**Table 7. Test 622 Run 154- Forced Transition x/c=0.05 Lower Surface.**

| Point | $C_T/\sigma$ | $C_P$ | FM | $\theta_{0.75}$ | $M_{tip}$ | TA | PA | $\rho$ |
|---|---|---|---|---|---|---|---|---|
| - | - | - | - | deg | - | degF | psf | $slug/ft^3$ |
| 1275 | 0.034 | 0.000285 | 0.523 | 7.05 | 0.584 | 84.10 | 2124.88 | 0.00226 |
| 1276 | 0.042 | 0.000342 | 0.583 | 7.97 | 0.584 | 84.09 | 2124.88 | 0.00226 |
| 1277 | 0.050 | 0.000417 | 0.637 | 8.96 | 0.584 | 84.12 | 2124.88 | 0.00226 |
| 1278 | 0.058 | 0.000486 | 0.671 | 9.77 | 0.584 | 84.16 | 2124.88 | 0.00226 |
| 1279 | 0.066 | 0.000566 | 0.702 | 10.63 | 0.584 | 84.30 | 2124.68 | 0.00226 |
| 1280 | 0.073 | 0.000645 | 0.722 | 11.43 | 0.584 | 84.46 | 2124.88 | 0.00226 |
| 1281 | 0.082 | 0.000749 | 0.741 | 12.34 | 0.584 | 84.60 | 2124.88 | 0.00225 |
| 1282 | 0.089 | 0.000831 | 0.749 | 13.03 | 0.584 | 84.82 | 2124.88 | 0.00225 |
| 1283 | 0.095 | 0.000913 | 0.757 | 13.63 | 0.583 | 85.07 | 2124.88 | 0.00225 |
| 1284 | 0.098 | 0.000946 | 0.758 | 13.89 | 0.583 | 85.29 | 2124.88 | 0.00225 |
| 1285 | 0.093 | 0.000880 | 0.755 | 13.40 | 0.583 | 85.46 | 2124.68 | 0.00225 |
| 1286 | 0.084 | 0.000772 | 0.744 | 12.53 | 0.583 | 85.57 | 2124.68 | 0.00225 |
| 1287 | 0.076 | 0.000674 | 0.730 | 11.67 | 0.583 | 85.59 | 2124.88 | 0.00225 |
| 1288 | 0.069 | 0.000592 | 0.711 | 10.91 | 0.583 | 85.59 | 2124.68 | 0.00225 |
| 1289 | 0.060 | 0.000504 | 0.682 | 9.98 | 0.583 | 85.55 | 2124.68 | 0.00225 |
| 1290 | 0.053 | 0.000438 | 0.652 | 9.20 | 0.583 | 85.51 | 2124.68 | 0.00225 |
| 1291 | 0.044 | 0.000363 | 0.604 | 8.23 | 0.583 | 85.45 | 2124.68 | 0.00225 |
| 1292 | 0.036 | 0.000296 | 0.539 | 7.26 | 0.583 | 85.38 | 2124.88 | 0.00225 |
| 1293 | 0.031 | 0.000259 | 0.488 | 6.58 | 0.583 | 85.30 | 2124.88 | 0.00225 |

American Institute of Aeronautics and Astronautics

**Table 8. Test 622 Run 156- Forced Transition x/c=0.05 Upper and Lower Surfaces.**

| Point | $C_T/\sigma$ | $C_P$ | FM | $\theta_{0.75}$ | $M_{tip}$ | TA | PA | $\rho$ |
|-------|--------------|-------|-----|-----------------|-----------|------|------|--------|
| - | - | - | - | deg | - | degF | psf | $slug/ft^3$ |
| 1301 | 0.030 | 0.000286 | 0.437 | 6.80 | 0.585 | 81.68 | 2126.14 | 0.00227 |
| 1302 | 0.038 | 0.000335 | 0.509 | 7.66 | 0.585 | 82.27 | 2126.14 | 0.00227 |
| 1303 | 0.046 | 0.000406 | 0.580 | 8.68 | 0.585 | 82.67 | 2126.14 | 0.00226 |
| 1304 | 0.053 | 0.000466 | 0.621 | 9.45 | 0.585 | 83.01 | 2125.93 | 0.00226 |
| 1305 | 0.062 | 0.000554 | 0.661 | 10.44 | 0.584 | 83.28 | 2126.14 | 0.00226 |
| 1306 | 0.070 | 0.000634 | 0.687 | 11.25 | 0.584 | 83.54 | 2125.93 | 0.00226 |
| 1307 | 0.079 | 0.000736 | 0.709 | 12.17 | 0.584 | 83.86 | 2125.93 | 0.00226 |
| 1308 | 0.085 | 0.000812 | 0.719 | 12.81 | 0.584 | 84.20 | 2125.93 | 0.00226 |
| 1309 | 0.093 | 0.000910 | 0.730 | 13.62 | 0.584 | 84.54 | 2125.93 | 0.00226 |
| 1310 | 0.096 | 0.000949 | 0.733 | 13.89 | 0.583 | 84.78 | 2125.93 | 0.00225 |
| 1311 | 0.088 | 0.000847 | 0.725 | 13.06 | 0.583 | 84.98 | 2125.93 | 0.00225 |
| 1312 | 0.080 | 0.000744 | 0.711 | 12.22 | 0.583 | 85.07 | 2125.93 | 0.00225 |
| 1313 | 0.072 | 0.000649 | 0.694 | 11.37 | 0.583 | 85.11 | 2125.93 | 0.00225 |
| 1314 | 0.064 | 0.000570 | 0.670 | 10.61 | 0.583 | 85.14 | 2125.93 | 0.00225 |
| 1315 | 0.056 | 0.000485 | 0.633 | 9.69 | 0.583 | 85.11 | 2125.93 | 0.00225 |
| 1316 | 0.047 | 0.000409 | 0.585 | 8.72 | 0.583 | 85.07 | 2125.93 | 0.00225 |
| 1317 | 0.040 | 0.000355 | 0.536 | 7.94 | 0.583 | 85.01 | 2125.93 | 0.00225 |
| 1318 | 0.032 | 0.000293 | 0.452 | 6.91 | 0.584 | 84.95 | 2125.93 | 0.00225 |

American Institute of Aeronautics and Astronautics

**Table 9. Test 622 Run 157- Forced Transition x/c=0.05 Upper and Lower Surfaces.**

| Point | $C_T/\sigma$ | $C_P$ | FM | $\theta_{0.75}$ | $M_{tip}$ | TA | PA | $\rho$ |
|-------|------|------|------|------|------|------|------|------|
| - | - | - | - | deg | - | degF | psf | $slug/ft^3$ |
| 1319 | 0.034 | 0.000304 | 0.473 | 7.12 | 0.584 | 84.89 | 2125.93 | 0.00225 |
| 1320 | 0.042 | 0.000365 | 0.548 | 8.12 | 0.584 | 84.85 | 2125.93 | 0.00225 |
| 1321 | 0.050 | 0.000438 | 0.605 | 9.11 | 0.583 | 84.89 | 2125.72 | 0.00225 |
| 1322 | 0.058 | 0.000506 | 0.646 | 9.93 | 0.584 | 84.96 | 2125.72 | 0.00225 |
| 1323 | 0.066 | 0.000584 | 0.677 | 10.77 | 0.583 | 85.04 | 2125.72 | 0.00225 |
| 1324 | 0.074 | 0.000670 | 0.701 | 11.60 | 0.583 | 85.20 | 2125.72 | 0.00225 |
| 1325 | 0.083 | 0.000785 | 0.720 | 12.60 | 0.583 | 85.38 | 2125.72 | 0.00225 |
| 1326 | 0.090 | 0.000861 | 0.731 | 13.21 | 0.583 | 85.61 | 2125.72 | 0.00225 |
| 1327 | 0.096 | 0.000947 | 0.738 | 13.87 | 0.583 | 85.83 | 2125.72 | 0.00225 |
| 1328 | 0.092 | 0.000895 | 0.733 | 13.48 | 0.583 | 86.01 | 2125.72 | 0.00225 |
| 1329 | 0.083 | 0.000781 | 0.723 | 12.55 | 0.583 | 86.12 | 2125.72 | 0.00225 |
| 1330 | 0.075 | 0.000688 | 0.707 | 11.74 | 0.583 | 86.16 | 2125.72 | 0.00225 |
| 1331 | 0.067 | 0.000597 | 0.684 | 10.90 | 0.583 | 86.17 | 2125.51 | 0.00225 |
| 1332 | 0.060 | 0.000525 | 0.660 | 10.12 | 0.583 | 86.14 | 2125.72 | 0.00225 |
| 1333 | 0.052 | 0.000455 | 0.620 | 9.36 | 0.583 | 86.11 | 2125.51 | 0.00225 |
| 1334 | 0.044 | 0.000384 | 0.571 | 8.40 | 0.583 | 86.06 | 2125.72 | 0.00225 |
| 1335 | 0.036 | 0.000322 | 0.503 | 7.45 | 0.583 | 85.97 | 2125.72 | 0.00225 |
| 1336 | 0.037 | 0.000332 | 0.513 | 7.60 | 0.583 | 85.90 | 2125.72 | 0.00225 |
| 1337 | 0.039 | 0.000344 | 0.528 | 7.80 | 0.583 | 85.86 | 2125.72 | 0.00225 |
| 1338 | 0.038 | 0.000338 | 0.522 | 7.70 | 0.583 | 85.83 | 2125.72 | 0.00225 |
| 1339 | 0.029 | 0.000277 | 0.430 | 6.61 | 0.583 | 85.79 | 2125.72 | 0.00225 |

American Institute of Aeronautics and Astronautics

**Table 10. Test 622 Run 158- Forced Transition x/c=0.05 Upper Surface.**

| Point | $C_T/\sigma$ | $C_P$ | FM | $\theta_{0.75}$ | $M_{tip}$ | TA | PA | $\rho$ |
|---|---|---|---|---|---|---|---|---|
| - | - | - | - | deg | - | degF | psf | $slug/ft^3$ |
| 1342 | 0.030 | 0.000276 | 0.446 | 6.73 | 0.584 | 83.86 | 2125.09 | 0.00226 |
| 1343 | 0.038 | 0.000329 | 0.529 | 7.69 | 0.584 | 84.29 | 2125.09 | 0.00226 |
| 1344 | 0.045 | 0.000387 | 0.588 | 8.56 | 0.584 | 84.61 | 2125.09 | 0.00226 |
| 1345 | 0.054 | 0.000456 | 0.640 | 9.46 | 0.583 | 84.89 | 2125.09 | 0.00225 |
| 1346 | 0.062 | 0.000530 | 0.677 | 10.34 | 0.583 | 85.09 | 2125.09 | 0.00225 |
| 1347 | 0.070 | 0.000621 | 0.706 | 11.25 | 0.583 | 85.31 | 2124.88 | 0.00225 |
| 1348 | 0.077 | 0.000701 | 0.721 | 11.99 | 0.583 | 85.51 | 2124.88 | 0.00225 |
| 1349 | 0.086 | 0.000798 | 0.736 | 12.80 | 0.583 | 85.73 | 2124.88 | 0.00225 |
| 1350 | 0.094 | 0.000912 | 0.745 | 13.69 | 0.583 | 86.01 | 2124.68 | 0.00225 |
| 1351 | 0.096 | 0.000939 | 0.747 | 13.85 | 0.583 | 86.21 | 2124.68 | 0.00225 |
| 1352 | 0.087 | 0.000814 | 0.739 | 12.93 | 0.583 | 86.42 | 2124.68 | 0.00225 |
| 1353 | 0.081 | 0.000739 | 0.731 | 12.31 | 0.583 | 86.53 | 2124.68 | 0.00225 |
| 1354 | 0.071 | 0.000628 | 0.707 | 11.31 | 0.583 | 86.56 | 2124.68 | 0.00225 |
| 1355 | 0.064 | 0.000551 | 0.684 | 10.52 | 0.582 | 86.57 | 2124.68 | 0.00225 |
| 1356 | 0.055 | 0.000469 | 0.649 | 9.62 | 0.583 | 86.53 | 2124.47 | 0.00225 |
| 1357 | 0.048 | 0.000403 | 0.605 | 8.77 | 0.583 | 86.50 | 2124.47 | 0.00225 |
| 1358 | 0.041 | 0.000347 | 0.555 | 7.98 | 0.583 | 86.43 | 2124.47 | 0.00225 |
| 1359 | 0.032 | 0.000287 | 0.474 | 6.97 | 0.583 | 86.39 | 2124.47 | 0.00225 |

American Institute of Aeronautics and Astronautics

**Table 11. Test 622 Run 159- Forced Transition x/c=0.05 Upper Surface.**

| Point | $C_T/\sigma$ | $C_P$ | FM | $\theta_{0.75}$ | $M_{tip}$ | TA | PA | $\rho$ |
|-------|------|------|------|------|------|------|------|------|
| - | - | - | - | deg | - | degF | psf | $slug/ft^3$ |
| 1360 | 0.034 | 0.000299 | 0.490 | 7.17 | 0.583 | 86.32 | 2124.47 | 0.00225 |
| 1361 | 0.042 | 0.000359 | 0.569 | 8.17 | 0.583 | 86.27 | 2124.47 | 0.00225 |
| 1362 | 0.050 | 0.000420 | 0.620 | 9.04 | 0.583 | 86.25 | 2124.47 | 0.00225 |
| 1363 | 0.058 | 0.000495 | 0.663 | 9.95 | 0.583 | 86.30 | 2124.47 | 0.00225 |
| 1364 | 0.067 | 0.000581 | 0.696 | 10.87 | 0.583 | 86.36 | 2124.47 | 0.00225 |
| 1365 | 0.074 | 0.000656 | 0.719 | 11.58 | 0.583 | 86.47 | 2124.47 | 0.00225 |
| 1366 | 0.081 | 0.000739 | 0.734 | 12.32 | 0.583 | 86.60 | 2124.47 | 0.00225 |
| 1367 | 0.090 | 0.000848 | 0.745 | 13.20 | 0.583 | 86.80 | 2124.47 | 0.00225 |
| 1368 | 0.094 | 0.000906 | 0.750 | 13.66 | 0.582 | 87.10 | 2124.47 | 0.00224 |
| 1369 | 0.092 | 0.000870 | 0.747 | 13.36 | 0.582 | 87.24 | 2124.47 | 0.00224 |
| 1370 | 0.084 | 0.000771 | 0.738 | 12.58 | 0.582 | 87.32 | 2124.47 | 0.00224 |
| 1371 | 0.076 | 0.000676 | 0.724 | 11.71 | 0.582 | 87.36 | 2124.26 | 0.00224 |
| 1372 | 0.066 | 0.000571 | 0.696 | 10.76 | 0.582 | 87.36 | 2124.26 | 0.00224 |
| 1373 | 0.061 | 0.000519 | 0.676 | 10.18 | 0.582 | 87.31 | 2124.26 | 0.00224 |
| 1374 | 0.050 | 0.000423 | 0.624 | 9.05 | 0.582 | 87.27 | 2124.26 | 0.00224 |
| 1375 | 0.044 | 0.000375 | 0.587 | 8.42 | 0.582 | 87.20 | 2124.26 | 0.00224 |
| 1376 | 0.036 | 0.000315 | 0.516 | 7.45 | 0.582 | 87.13 | 2124.26 | 0.00224 |
| 1377 | 0.030 | 0.000272 | 0.449 | 6.66 | 0.582 | 87.06 | 2124.26 | 0.00224 |